DTIC FILE COPY

(12)

AD-A188 212

TGAL-86-08

STUDIES IN DECOUPLING

I.N. Gupta, K.L. McLaughlin, R.A. Wagner, T.W. McElfresh, M.E. Marshall and R.S. Jih

Teledyne Geotech Alexandria Laboratories
314 Montgomery Street
Alexandria, Virginia 22314-1581

NOVEMBER 1986

ANNUAL REPORT:
ARPA ORDER NO: 4435
PROJECT TITLE: Miscellaneous Discrimination Studies
CONTRACT: F08606-85-C-0022

Prepared for:
DEFENSE ADVANCED RESEARCH PROJECTS AGENCY
1400 Wilson Boulevard
Arlington, VA 22209

Monitored By:
AFTAC/TGR
PATRICK AFB
FLORIDA 32925-6001

87 11 03 158

UNCLASSIFIED
SECURITY CLASSIFICATION OF THIS PAGE

A13 8212

REPORT DOCUMENTATION PAGE

Form Approved
OMB No 0704-0188
Exp Date Jun 30, 1986

1a REPORT SECURITY CLASSIFICATION Unclassified	1b RESTRICTIVE MARKINGS
2a SECURITY CLASSIFICATION AUTHORITY 2b DECLASSIFICATION / DOWNGRADING SCHEDULE	3 DISTRIBUTION / AVAILABILITY OF REPORT Approved for Public Release; Distribution Unlimited.
4 PERFORMING ORGANIZATION REPORT NUMBER(S) TGAL-86-8	5 MONITORING ORGANIZATION REPORT NUMBER(S)
6a NAME OF PERFORMING ORGANIZATION Teledyne Geotech Alexandria Laboratories 6b OFFICE SYMBOL (If applicable)	7a NAME OF MONITORING ORGANIZATION AFTAC/TGR
6c ADDRESS (City, State, and ZIP Code) 314 Montgomery Street Alexandria, VA 22314	7b ADDRESS (City, State, and ZIP Code) Patrick Air Force Base Florida 32925-6001
8a NAME OF FUNDING / SPONSORING ORGANIZATION DARPA 8b OFFICE SYMBOL (If applicable) GSD	9 PROCUREMENT INSTRUMENT IDENTIFICATION NUMBER F08606-85-C-0022
8c ADDRESS (City, State, and ZIP Code) 1400 Wilson Blvd. Arlington, VA 22209	10 SOURCE OF FUNDING NUMBERS PROGRAM ELEMENT NO: 62714E PROJECT NO: TASK NO: WORK UNIT ACCESSION NO:

11 TITLE (Include Security Classification)
Studies in Decoupling

12 PERSONAL AUTHOR(S)
I.N. Gupta, K.L. McLaughlin, R.A. Wagner, T.W. McElfresh, M.E. Marshall, R.S. Jih

13a TYPE OF REPORT	13b TIME COVERED	14 DATE OF REPORT (Year, Month, Day)	15 PAGE COUNT
Annual Report	FROM Mar 85 TO Sep 87	November 1986	79

16 SUPPLEMENTARY NOTATION

17 COSATI CODES			18 SUBJECT TERMS (Continue on reverse if necessary and identify by block number)
FIELD	GROUP	SUB-GROUP	
08	11		Decoupling; Scaled depth; regional phases; strain and frequency-dependent Q; Lg
17	10		

19 ABSTRACT (Continue on reverse if necessary and identify by block number)

SECTION A

An understanding of the frequency dependence of decoupling is essential for monitoring nuclear explosions detonated in large underground cavities. Analysis of available data from the nuclear explosions Salmon (5.3 kt in salt) and Sterling (0.38 kt shot in the cavity created by Salmon) recorded at shot-receiver distances of 16, 32, and 27 km, confirmed the earlier findings of Blandford and Woolson (1979) indicating: (1) reduced decoupling of Sterling at higher frequencies for both P and "Lg," and (2) relatively greater decoupling of Sterling for Lg than for P at high frequencies. In an attempt to understand why the frequency dependence of the decoupling ratio is different for P and the Lg group, we examined the spectral content of Pn and Lg from 7 Pahute Mesa, NTS explosions covering a wide range of scaled depths and

20 DISTRIBUTION / AVAILABILITY OF ABSTRACT ☐ UNCLASSIFIED/UNLIMITED ☒ SAME AS RPT ☐ DTIC USERS	21 ABSTRACT SECURITY CLASSIFICATION Unclassified
22a NAME OF RESPONSIBLE INDIVIDUAL Dr. Dean Clauter	22b TELEPHONE (Include Area Code) (305) 494-5236 22c OFFICE SYMBOL TGR

DD FORM 1473, 84 MAR — 83 APR edition may be used until exhausted. All other editions are obsolete

SECURITY CLASSIFICATION OF THIS PAGE
UNCLASSIFIED

(19 Continued)

recorded at a common station, KN-UT. The spectral ratio Pn/Lg varied strongly with scaled depth, mainly due to significantly greater dependence on scaled depth of the spectra of Pn than of Lg. These results are in agreement with those from Salmon and Sterling with scaled depths of 475 and 1145 m/(kt)$^{1/3}$, respectively. A possible reason for the decoupling at higher frequencies to be different for P and Lg is therefore the greater scaled depth of decoupled shots. The larger variability of Pn spectra than those of Lg can be due to an explosion (especially those that are not overburied) approximating a pressurized ellipsoid cavity with major axis in the vertical direction so that the source function is more variable for down-going waves comprising Pn than for others making up Lg. The spectral ratio Pn/Lg may be useful in discriminating between decoupled (or overburied) and normal shots.

SECTION B

The amplitude and spectra of teleseismic and regional seismic P waves depend on the material properties in the source region. The effects of strain and frequency dependent attenuation are therefore important for understanding the source characteristics of coupled versus decoupled explosions. Near-field velocity and acceleration data from the Salmon and Sterling explosions in salt were analyzed for strain and frequency dependent attenuation. Attenuation, parameterized as 1/Q, was estimated for various source-receiver distance ranges and frequency bandwidths by using two methods: (a) mean spectral ratio slope and (b) average amplitude spectral ratio. Results from Salmon indicate that (1) in the frequency range of 1-25 Hz, Q is about 5 to 10; (2) Q increases with source-receiver distance, suggesting lower Q for larger strain levels; (3) Q in the frequency range of 25-50 Hz is substantially higher than in the frequency range of 1-25 Hz, or Q increases with frequency. Analysis of data from Sterling indicates that Q is frequency independent and about one order of magnitude larger than for Salmon. Therefore the near-source attenuation was strain and frequency dependent and hence non-linear for Salmon out to a range of 600 m.

This report contains studies on

SECTION A

A STUDY OF SEISMIC DECOUPLING USING SALMON, STERLING, AND PAHUTE MESA nuclear EXPLOSIONS, and on strain and frequency dependent attenuation estimates in salt from Salmon and Sterling near-field recordings.

SUMMARY

An understanding of the frequency dependence of decoupling is essential for monitoring nuclear explosions detonated in large underground cavities. Analysis of available data from the nuclear explosions Salmon (5.3 kt in salt) and Sterling (0.38 kt shot in the cavity created by Salmon) recorded at shot-receiver distances of 16, 32, and 27 km, confirmed the earlier findings of Blandford and Woolson (1979) indicating: (1) reduced decoupling of Sterling at higher frequencies for both P and "Lg," (use single quotes) and (2) relatively greater decoupling of Sterling for Lg than for P at high frequencies. In an attempt to understand why the frequency dependence of the decoupling ratio is different for P and the Lg group, we examined the spectral content of Pn and Lg from 7 Pahute Mesa, NTS explosions covering a wide range of scaled depths and recorded at a common station, KN-UT. The spectral ratio Pn/Lg varied strongly with scaled depth, mainly due to significantly greater dependence on scaled depth of the spectra of Pn than of Lg. These results are in agreement with those from Salmon and Sterling with scaled depths of 475 and 1145 m/(kt)$^{1/3}$, respectively. A possible reason for the decoupling at higher frequencies to be different for P and Lg ~~is therefore~~ may be the greater scaled depth of decoupled shots. The larger variability of Pn spectra than those of Lg can be due to an explosion (especially those that are not overburied) approximating a pressurized ellipsoid cavity with major axis in the vertical direction so that the source function is more variable for down-going waves comprising Pn than for others making up Lg. The spectral ratio Pn/Lg may be useful in discriminating between decoupled (or overburied) and normal shots.

(THIS PAGE INTENTIONALLY LEFT BLANK)

TABLE OF CONTENTS

SECTION A

SECTION B

LIST OF FIGURES

INTRODUCTION

Most specialists on seismic verification are in agreement that the detonation of nuclear explosions in very large cavities represents the most significant evasion possibility (Sykes, 1987). Cavity decoupling will significantly challenge Comprehensive Test Ban Treaty (CTBT) verification of explosions near 1 kt, even with 30 in-country array stations (Hannon, 1986). The largest seismic arrivals recorded by these arrays will be the crustal wave guide phases such as Lg. It is therefore important to understand the differences in the generation of P and Lg by decoupled and tamped explosions. In their analysis of Salmon and Sterling data, Blandford and Woolson (1979) observed decoupling to vary as a function of frequency and the frequency dependence was substantially different for P and Lg. Their findings were, however, essentially based on data from a single station. One principal objective of this investigation was to verify their results by analyzing data from other stations and possibly to determine why decoupling varied with wave type.

The decoupled nuclear explosion Sterling (December 3, 1966) with yield of 0.38 kt and shot depth of 829 m was shot in the cavity of the nuclear explosion, Salmon (October 22, 1964) with a yield of 5.3 kt and shot depth of 828 m. Sterling was preceded by a high-explosive (HE) calibration shot (November 17, 1966), referred to hereafter as "Stercal", with yield equivalent to 2.7 tons of TNT, about 348 m from the Sterling location and at about the same depth, 831 m (Springer et al., 1968). The three explosions were recorded at several stations at varying distances and azimuths (see Figure 1 and Table 1 in Springer et al., 1968). The instrument responses as well as several examples of recordings can be seen in Springer et al. (1968) and Blandford and Woolson (1979). In this part of the study, we analyzed data primarily from the USCGS stations 10S and 20S (16 and 32 km south of shot point) since data from all other stations had already been examined in earlier studies. We used the spectral ratio method in which the spectra of observed signals from various sources, after correction for noise, are compared at common stations. Care was taken to use only those data that were free from spikes as well as clipped signals.

ANALYSIS OF DATA FROM STATION 10S

We first analyzed the Salmon, Sterling, and Stercal data at the USCGS station 10S located about 10 miles or 16 km south of ground-zero. Three-component broadband recordings of the three explosions at one of several receiver positions at this location can be seen in Springer et al. (1968, Figure 5). Among the digitized data available to us, at common sensors, only the vertical component data were found to be usable. The best quality data with high signal (S) to noise (N) ratio at station 10S for the three explosions were obtained at the receiver location C 2000; these are shown in Figure 1 in which the first P motions are aligned. On each record, the P waves are followed by larger-amplitude, lower frequency waves, starting about 1.7 sec after the onset of P. On the basis of available three-component data from Salmon, Sterling, and Stercal at comparable source-receiver distances in Borcherdt, et al. (1967), this prominent arrival is too early to be the direct S wave. In fact, synthetic seismograms based on source-receiver distance, $\Delta = 16$ km and crustal structure appropriate for this region, indicate this arrival to be due to mostly P waves reverberating in the low-velocity sediments and the S waves to arrive about 3.5 sec after P (Charles Langston, written communication). The records in Figure 1 indicate a prominent arrival with its beginning, denoted by S, about 3.3 sec after the first P and prominent on all three records. Following Blandford and Woolson (1969), we designate this group of waves as Lg. In spite of repeated attempts, the data could not be calibrated correctly; however, as we shall see later, this did not adversely affect most results in this study.

The term Lg is generally used to describe the prominent regional phase consisting of higher-mode surface waves (Knopoff et al., 1973). Equivalently, Lg may also be considered to be guided shear waves incident on the Moho at angles more grazing than the critical incidence and multiply reflected within the crust (Bouchon, 1982). It is therefore not proper to refer to

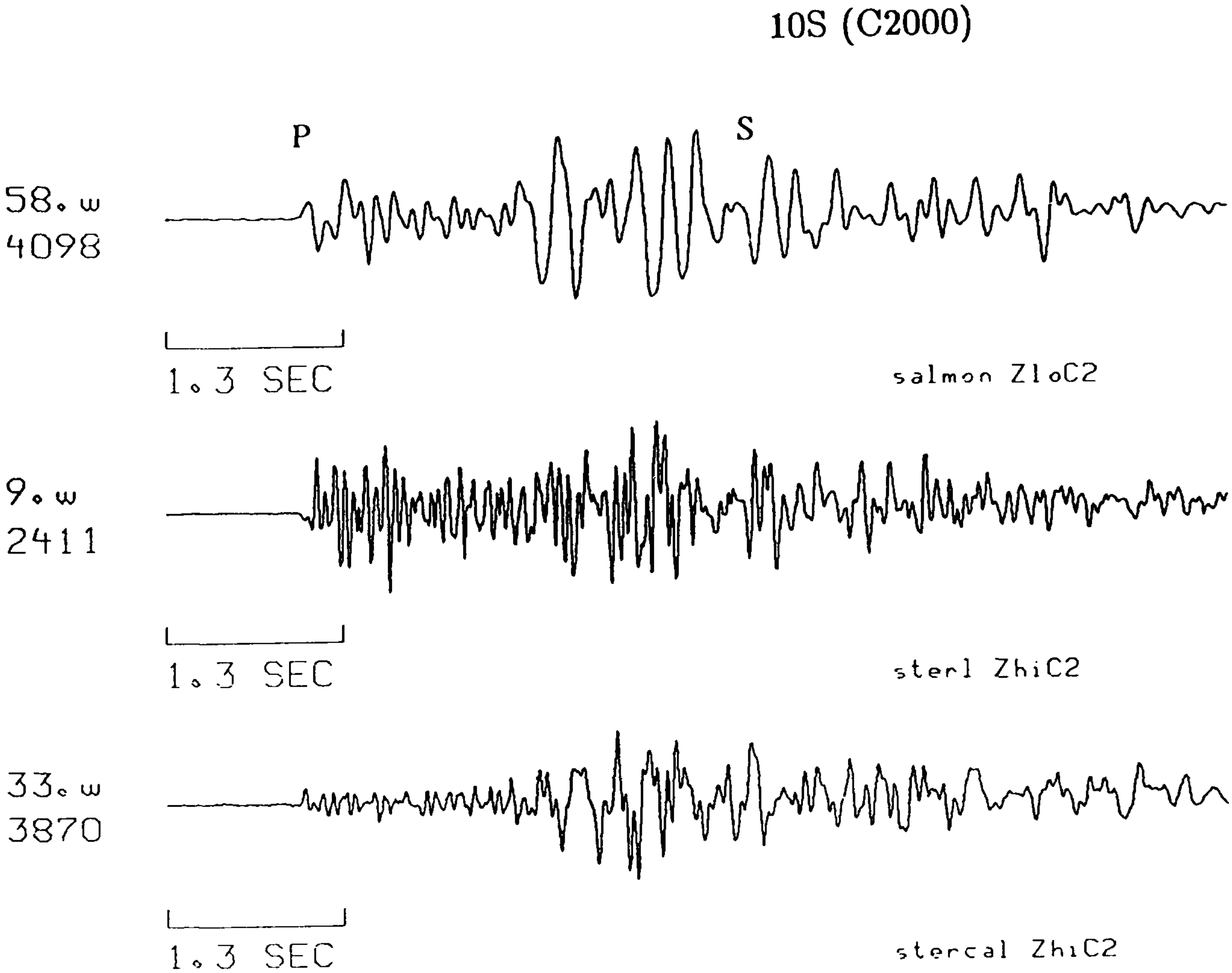

Figure 1. Raw common-receiver vertical component data recorded at station 10S (Receiver location C2000) for the three explosions Salmon, Sterling, and Stercal. The beginnings of the P and Lg wavetrains, indicated by the letters P and S, are separated by about 3.3 sec.

such waves as Lg at source-receiver distances of a few tens of km. The crustal structure in the vicinity of Salmon is however characterized by 3.1 to 3.7 km thick coastal sediments (average P-wave velocity 3 km/sec) overlying a layer with velocity of 5 km/sec associated with strong refraction arrivals (Warren et al., 1966). This provides sufficient impedance contrast for the upper low velocity layer to act as an efficient waveguide, giving rise to large-amplitude waves in the same manner as Lg. The numerical modeling of Lg by Campillo et al. (1985, see their Figures 9 and 10) also show that, for a shallow source, rays which contribute to the Lg wavetrain include those that are supercritically reflected on the upper, shallower discontinuities of the crust. We shall therefore retain the use of the term "Lg" to describe the low-frequency, large-amplitude waves such as those observed at the station 10S.

The digitization rate for the data in Figure 1 was 125 samples per sec. For each record, the initial P window is taken to be about 1 sec long (actually 128 points), a 10% cosine taper applied and the amplitude spectra are obtained over the frequency range of 0 to 50 Hz. This procedure, the same as used by Blandford and Woolson (1979) in their analysis of Salmon/Sterling data, was adopted so that the results in the two studies can be directly compared. A similar procedure was used for obtaining the spectra of Lg windows which were about 2 sec long (256 points); the starting points on the P and Lg windows were separated by about 1.6 sec. These spectra, with 3 and 5 point smoothing for P and Lg, respectively, are shown in Figures 2, 3, and 4 for Salmon, Sterling, and Stercal, respectively. These figures include similar spectra of samples of noise prior to the onset of P. The S/N ratio for Salmon appears to be good only up to about 25 Hz whereas for Sterling and Stercal S/N is good for somewhat higher frequencies.

The decoupling factor is defined as the ratio of the P-wave amplitude of a tamped explosion to that of the decoupled shot when the two explosions have the same yield. Since Salmon

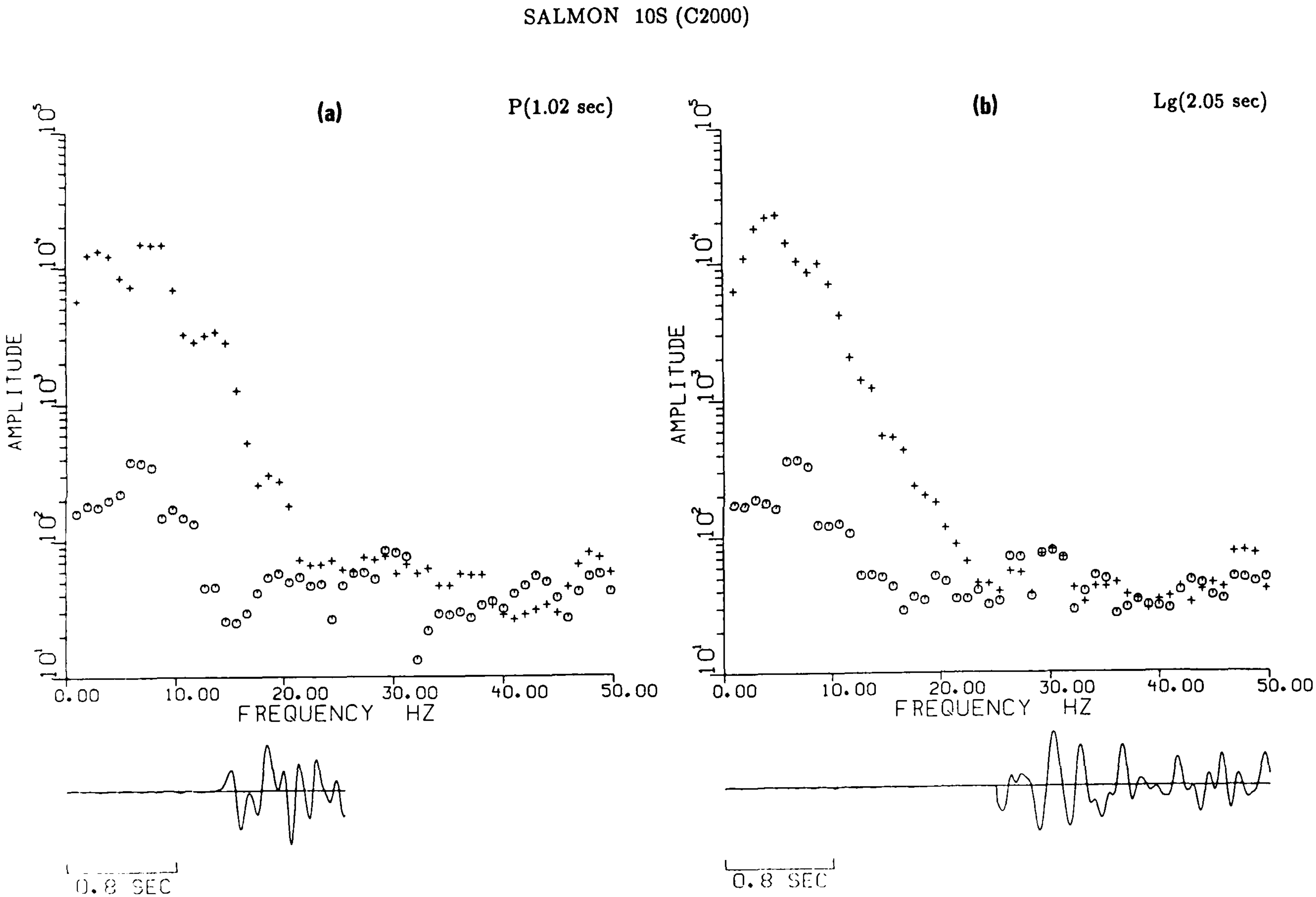

Figure 2. Spectra of the observed (a) P (window 1.02 sec long) and (b) Lg (window 2.05 sec long) for Salmon recorded at 10S. The spectra of noise preceding the onset of direct P are also shown. The amplitude values are in arbitrary units.

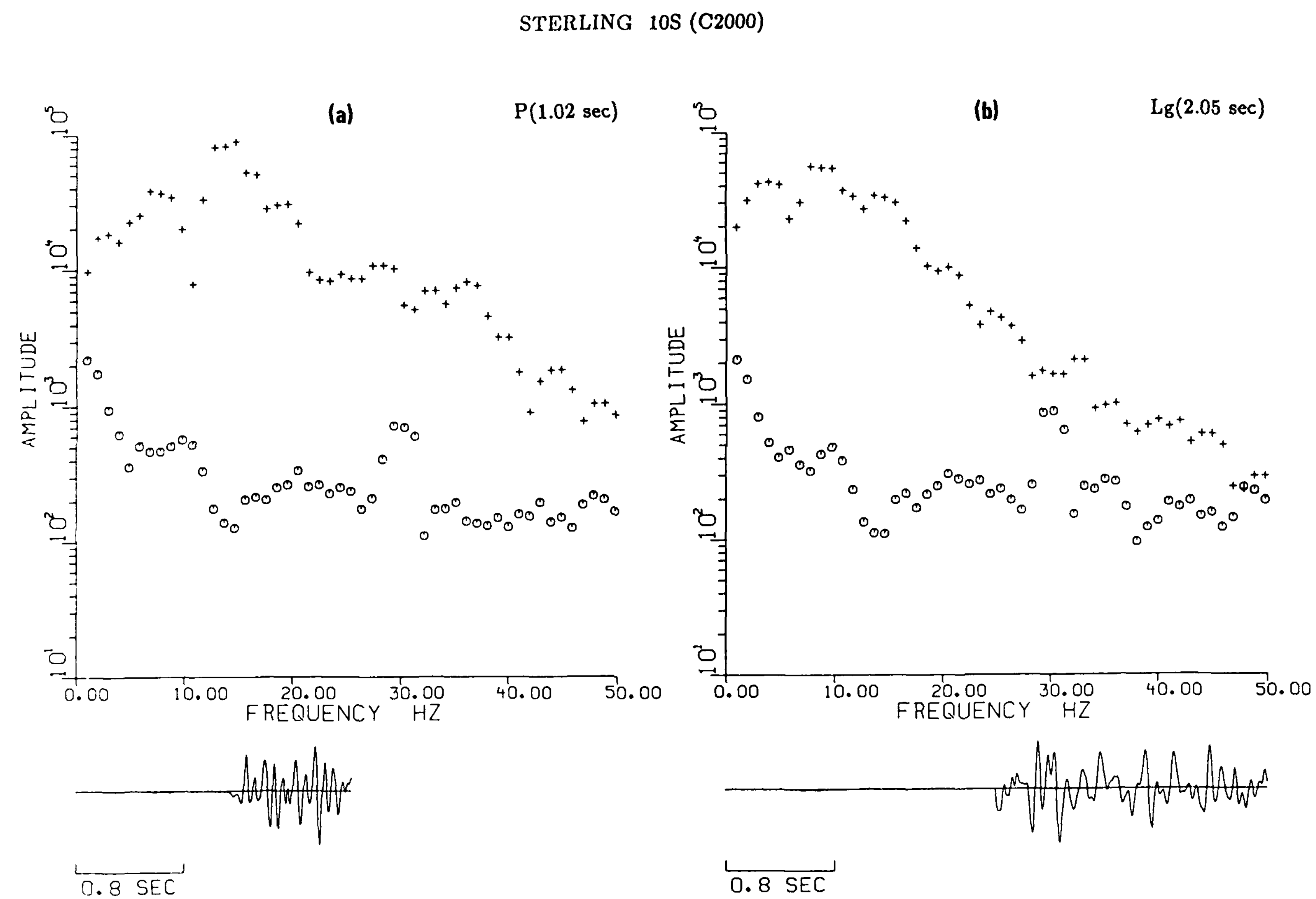

Figure 3. Spectra of the observed (a) P (window 1.02 sec long) and (b) Lg (window 2.05 long) for *Sterling* recorded at 10S. The spectra of noise preceding the onset of direct P are also shown. The amplitude values are in arbitrary units.

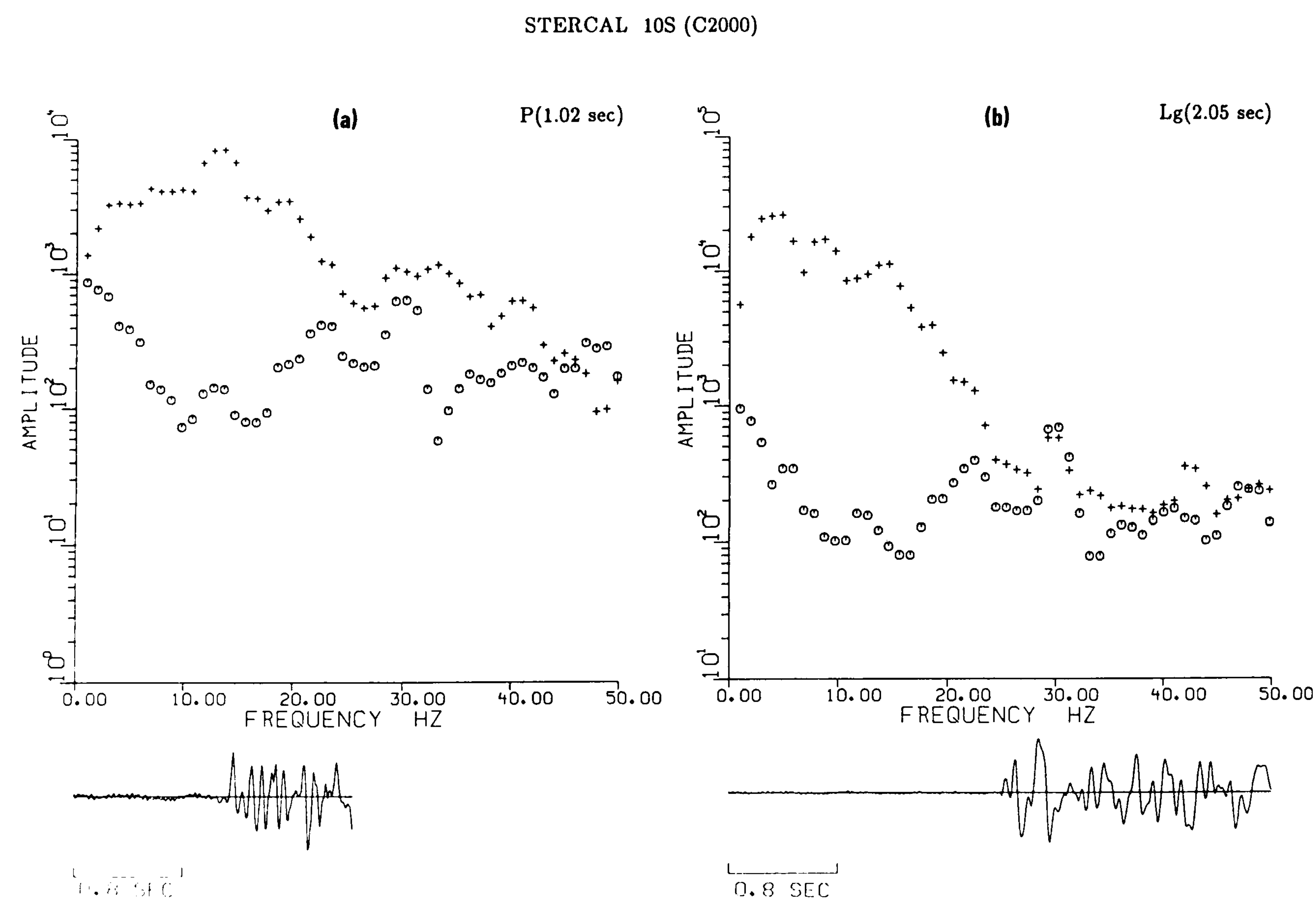

Figure 4. Spectra of the observed (a) P (window 1.02 sec long) and (b) Lg (window 2.05 sec long) for Stercal recorded at 10S. The spectra of noise preceding the onset of direct P are also shown. The amplitude values are in arbitrary units.

and Sterling had quite different yields, one needs to divide the observed Salmon/Sterling ratio at a given frequency by the theoretical spectral ratio of a 5.3 kt (Salmon) explosion to a 0.38 kt (Sterling tamped) explosion. We obtained the theoretical spectral ratios by using the von Seggern and Blandford (1972) source function for salt (i.e. k = 26 at 5 kt and B = 0). The source functions for explosions with yields of 5.3, 0.38, and 0.0027 kt, shown in Figure 5, have corner frequencies (half-amplitude points) at about 4, 10, and 50 Hz, respectively. The corresponding spectral ratios, shown in Figure 6, indicate considerable variation with frequency. The Salmon/Sterling ratio has values of approximately 14 and 3 at frequency of 1 and 20 Hz, respectively, whereas Sterling/Stercal ratio is approximately 140 and 30 at frequencies of 1 and 20 Hz, respectively. This means that, over the frequency range of 1 to 20 Hz, each of the theoretical ratios Salmon/Sterling(tamped) and Sterling(tamped)/Stercal decreases by a factor of $14/3 \approx 5$. Note that Springer et al.'s (1968, see especially their Figure 17) theoretical scaling of Salmon and Sterling spectra would indicate nearly the same results as in Figure 6.

The spectral ratios Salmon/Sterling, based on P and Lg windows containing 128 (1.02 sec) and 256 points (2.05 sec), respectively, for each shot and recorded at the same common vertical component location C 2000, are shown in Figures 7a and 7b, respectively. The amplitude ratio scales are obviously in error (because the data were uncalibrated) but an approximately correct scale was derived by comparing the station 10S amplitudes in Springer et al. (1968) with those in the digitized data; these are indicated at the left. The spectral ratios are corrected for noise and only those points for which the S/N power ratio is greater than 2 for each signal are included and the dashed line shows the mean (least squares) slope over the frequency range of 5.0 to 25.0 Hz. The spectral ratio for P drops at a fall-off rate of about $f^{-3.74}$ over the frequency range of 5 to 25 Hz. This fall-off rate is considerably faster than about f^{-2} expected on the basis of the source functions in Figure 6. The spectral ratio for Lg, shown in

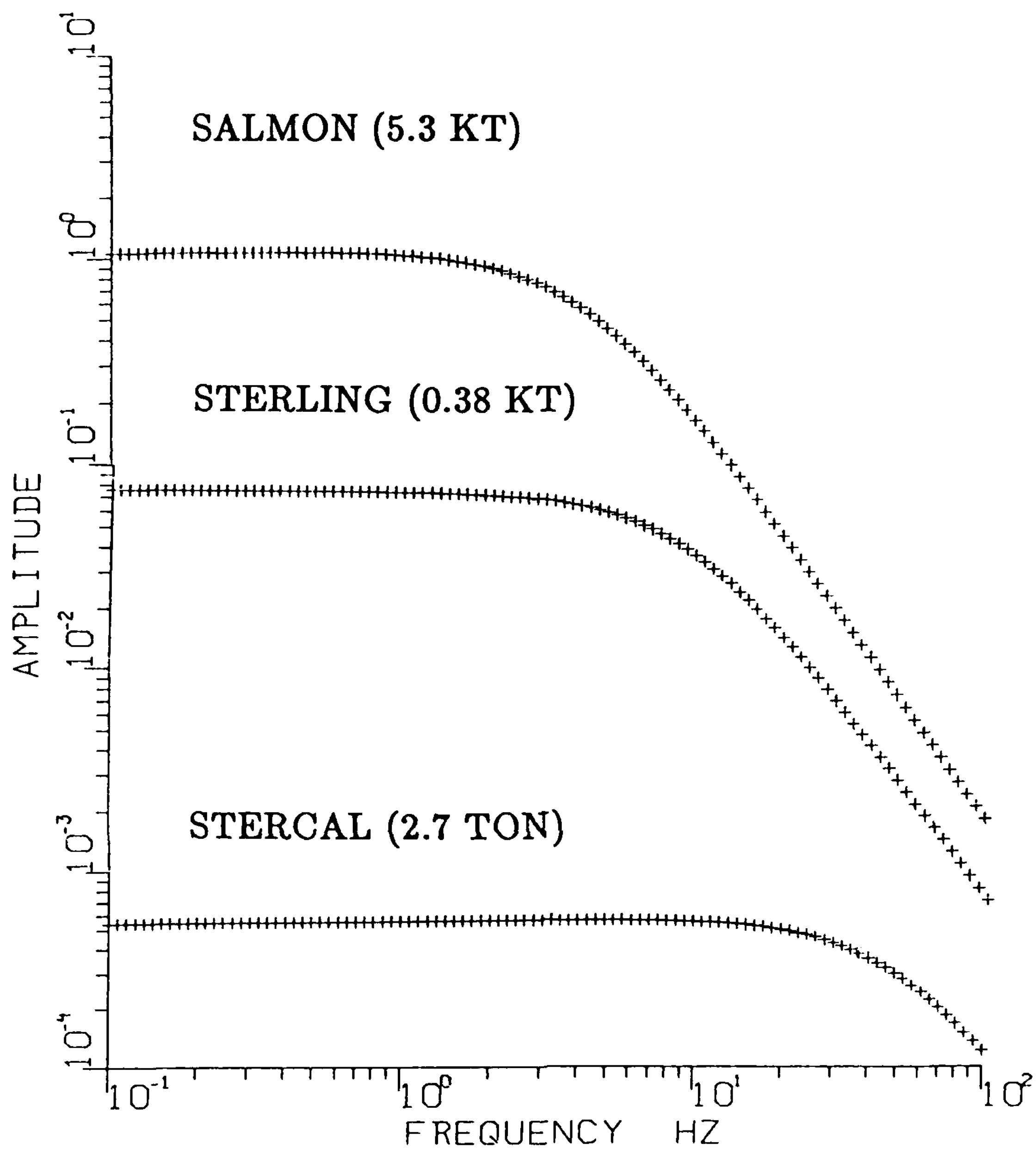

Figure 5. Theoretical spectra, based on von Seggern and Blandford's (1972) source function for salt, for yields of 5.3, 0.38, and 0.0027 kt, respectively. The corner frequencies (half amplitude points) for the three spectra are at about 4, 10, and 50 Hz, respectively.

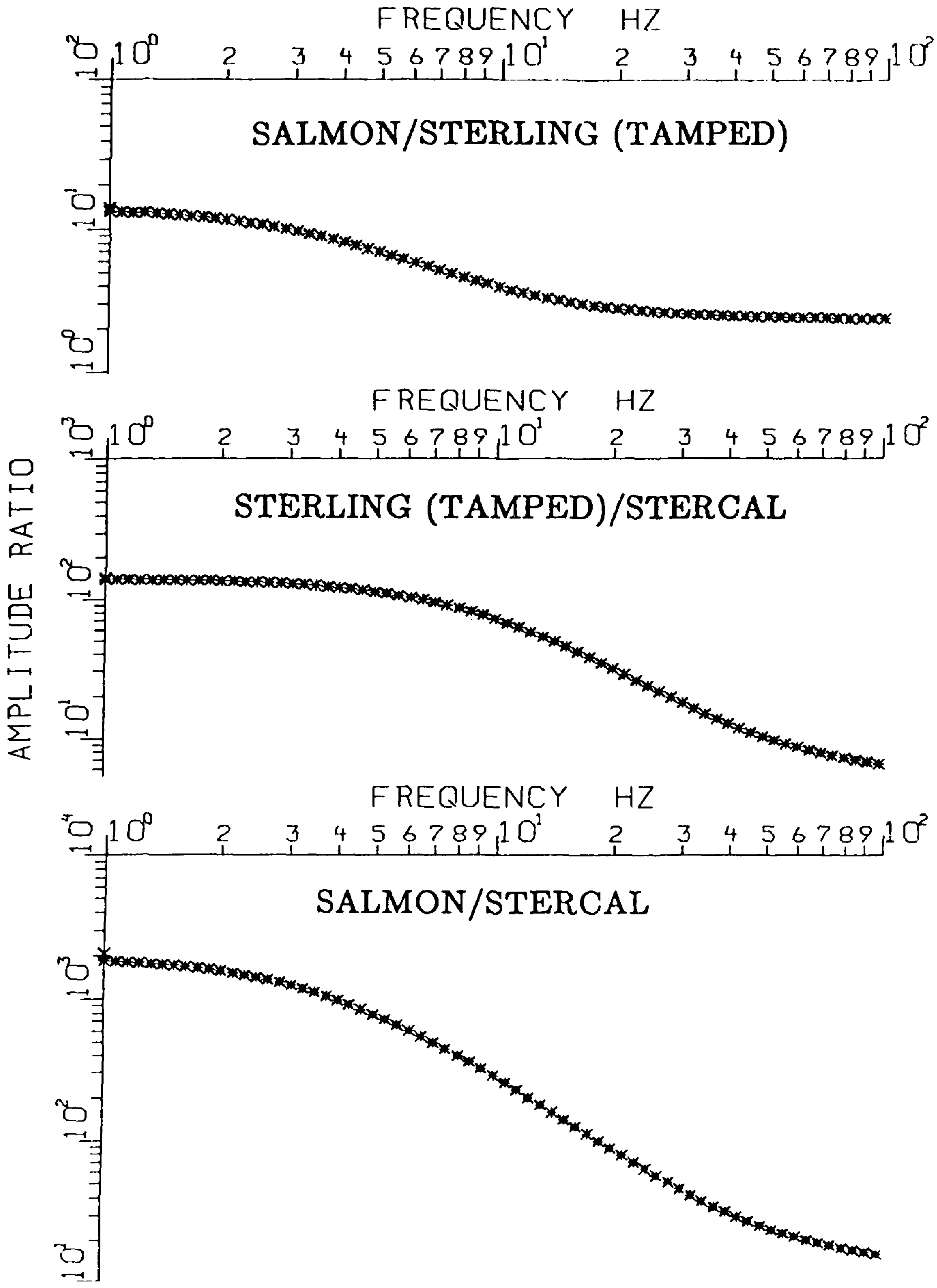

Figure 6 Theoretical spectral ratios for Salmon/Sterling (tamped), Sterling (tamped)/Stercal, and Salmon/Stercal over the frequency range 1 to 100 Hz.

SALMON/STERLING 10S (C2000)

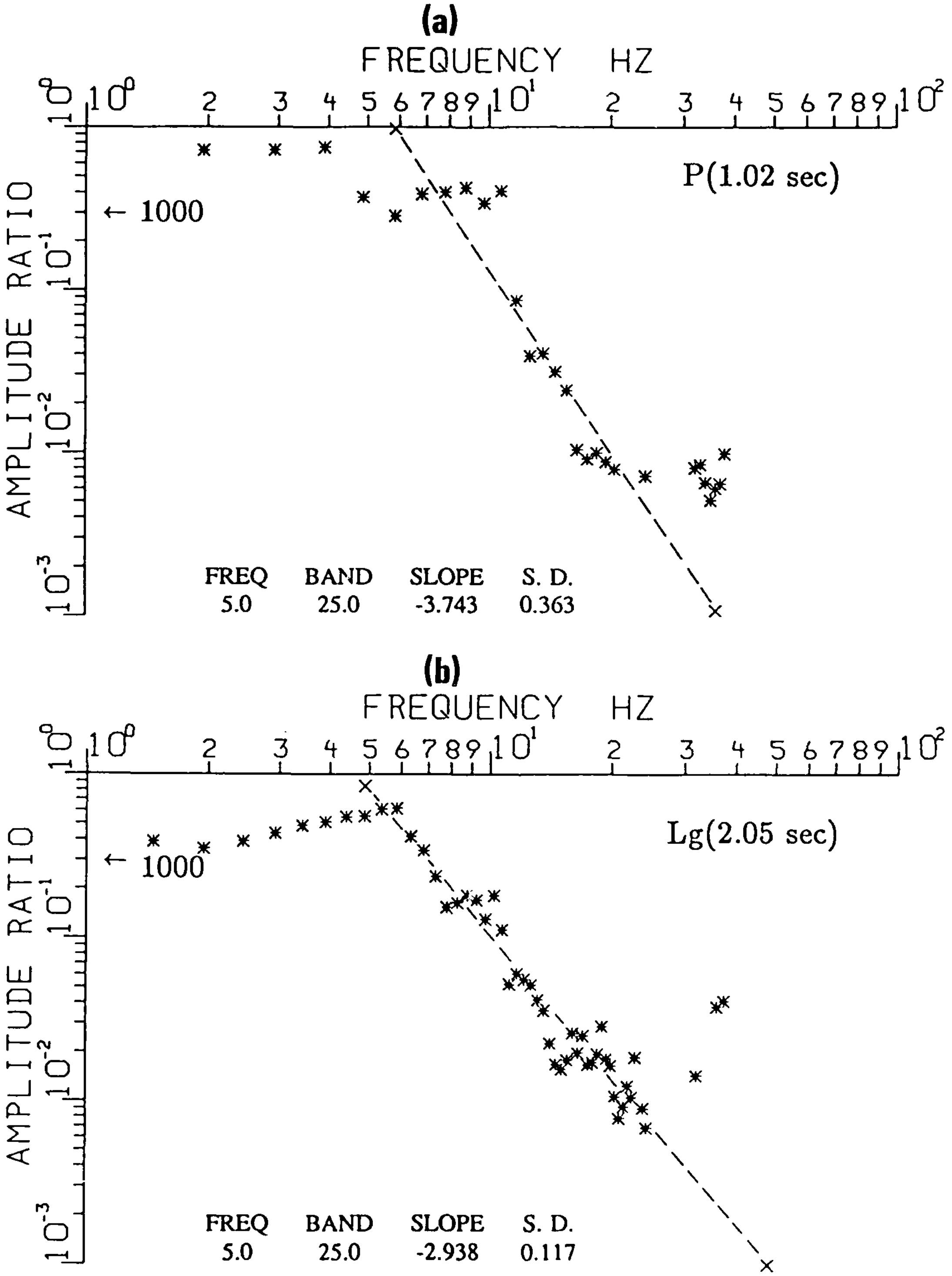

Figure 7. Spectral ratio Salmon/Sterling, corrected for noise, with logarithmic frequency scale, for (a) P window 1.02 sec long, and (b) Lg window 2.05 sec long. The dashed lines show mean (least squares) slopes over the frequency range 5 to 25 Hz. The mean value of slope and its standard deviation (S.D.) are indicated.

Figure 7b, indicate a fall-off rate of about $f^{-2.94}$, considerably smaller than that for P, over the frequency range 5 to 25 Hz. The P amplitude ratio (Figure 7a) drops by a factor of about 2000/30 ≈ 70 between 5 and 20 Hz. Similarly, in Figure 7b, the Lg amplitude ratio drops by a factor of about 2000/50 ≈ 40 between 5 and 20 Hz. Thus, at higher frequencies, the Sterling Lg is more decoupled than the Sterling P wave. The amplitude ratios at low frequencies and the significantly different fall-off rates for P and Lg are similar to those obtained by Blandford and Woolson (1979, see their Figure 15).

The observed spectral ratios for P in Figure 7(a) suggest the Salmon/Sterling ratios to be about 2000 and 30 at frequencies of 1 Hz (i.e. low-frequency value) and 20 Hz, respectively. The corrected decoupling factors for Salmon/Sterling are therefore 2000/14 ≈ 140 and 30/3 = 10, at frequencies of 1 and 20 Hz, respectively. The Sterling decoupling ratio for P is therefore reduced by a factor of 14 over the frequency range of 1 to 20 Hz. Similarly, on the basis of Figure 7b, the corrected decoupling factors for Lg are approximately 140 and 17 at frequencies of 1 and 20 Hz, respectively, and the decoupling ratio is reduced by a factor of only about 8 over the frequency range of 1 to 20 Hz.

The spectral ratios P/Lg for the three explosions, again from the same common vertical component location and corrected for noise, are shown in Figure 8. Note the similar spectral modulations in the three plots for frequencies up to about 20 Hz; this is probably because the source-receiver paths are almost identical in the three cases. Comparing the results for Salmon and Sterling, the differences in the two spectral ratios exist primarily at the higher frequencies. The dashed lines in Figure 8 show the mean (least squares) slopes over the frequency range of 5 to 25 Hz. For each explosion, the mean spectral slope values with its standard deviation (S. D.) are indicated for frequency bands of 5 to 25 Hz and 5 to 40 Hz. The mean slope values are significantly different for Salmon and Sterling and are the smallest for Salmon and the largest for Stercal.

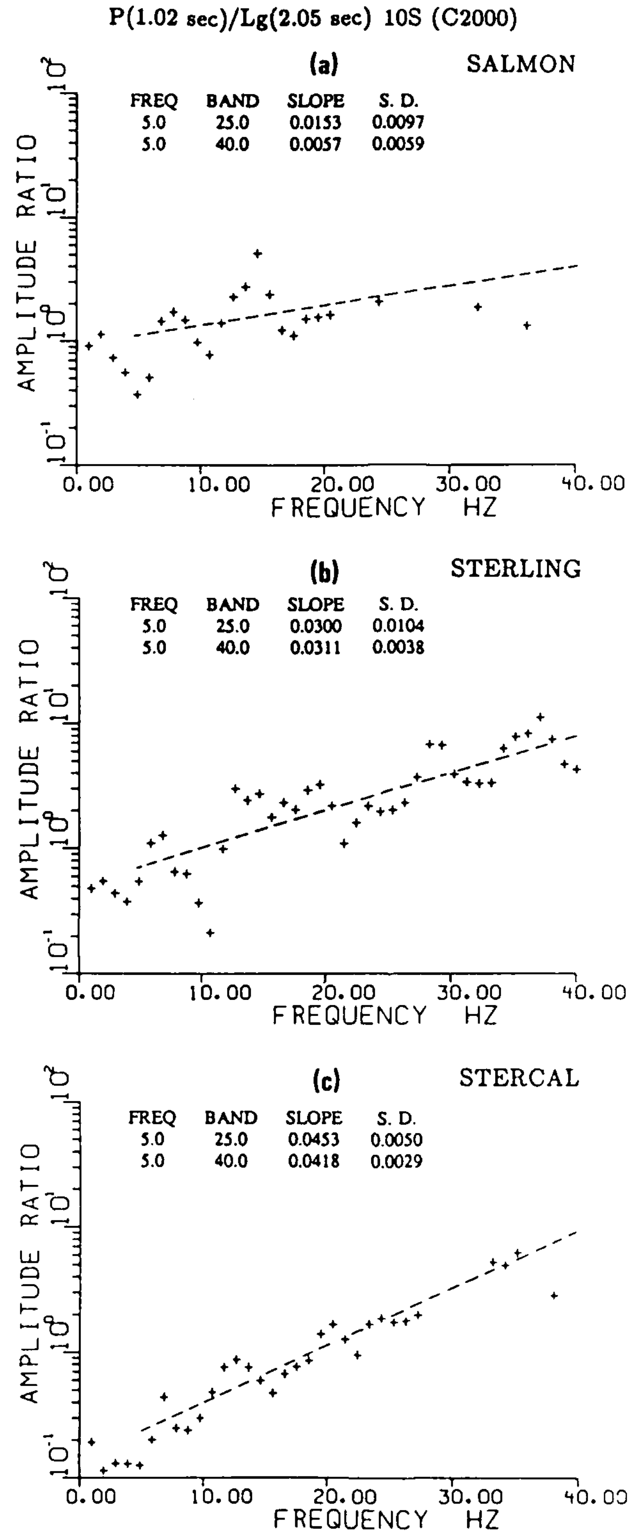

Figure 8. Spectral ratio P/Lg, corrected for noise, for (a) Salmon, (b) Sterling and (c) Stercal recorded at the station 10S. Points for which S/N power ratio is less than 2 are not plotted. The dashed lines show mean (least squares) slopes over the frequency range 5 to 25 Hz. The mean value of slope/Hz and its standard deviation (S.D.) are indicated for frequency ranges of 5 to 25 Hz and 5 to 40 Hz.

ANALYSIS OF DATA FROM STATION 20S

Recordings at the station 20S, located about 20 miles or 32 km south-southwest of the ground-zero, provided vertical component data with good S/N for both Salmon and Sterling. Nearly 24 sec of common-receiver data are shown in Figure 9 in which, similar to Figure 1, the P waves are followed by larger-amplitude, lower-frequency wave-packet, Lg, the onset of which is denoted by S. The beginnings of P and Lg are separated by about 5.5 sec which agrees well with the synthetics for $\Delta = 32$ km (Charles Langston, written communication). The spectra of P and noise windows, each 256 points (2.05 sec) long, for Salmon and Sterling, obtained in the same manner as for the data from station 10S, are shown in Figure 10. The spectral ratios Salmon/Sterling for P and Lg windows of lengths 256 and 512 points, respectively, are shown in Figure 11. Over the frequency range of 5 to 25 Hz, the amplitude ratios have fall-off rates of about $f^{-3.01}$ and $f^{-1.44}$ for P and Lg, respectively. The higher fall-off rate for the P ratio than for the Lg ratio is similar to the results obtained from the data at station 10S (Figure 7).

The spectral ratios P/Lg for Salmon and Sterling, corrected for noise, are shown in Figure 12. The spectral modulations for the two explosions are similar, especially at the lower frequencies. The differences in the spectral ratios lie mainly in their higher frequency values. The dashed lines, representing mean slope values over the frequency range of 5 to 25 Hz, show considerably smaller (more negative) slope for Salmon than for Sterling; the difference between the two slope values is 0.0414. All these results are similar to those for data from station 10S (Figure 8).

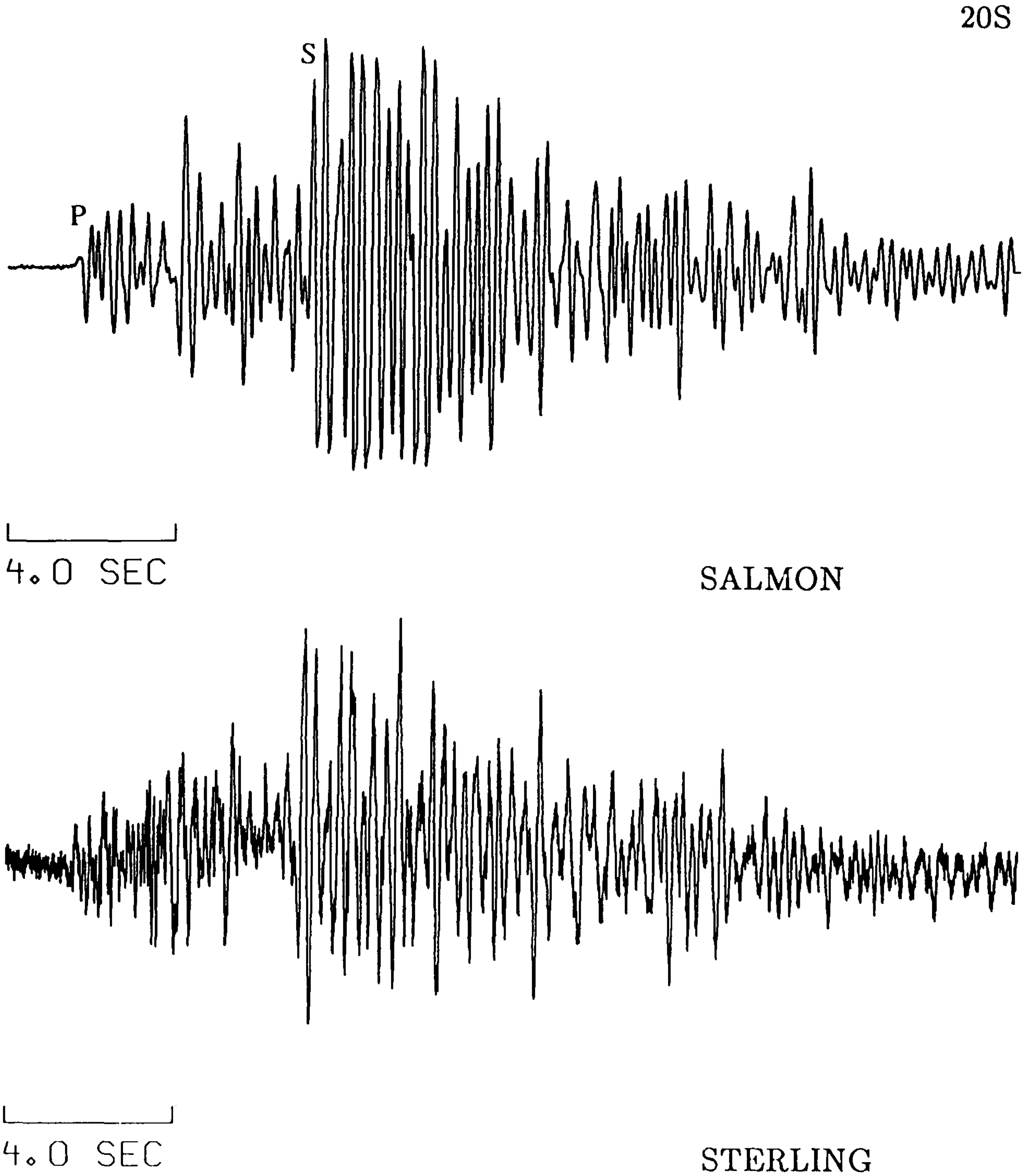

Figure 9. Raw common-receiver, vertical component data at station 20S for Salmon and Sterling. The beginnings of the P and Lg wavetrains, denoted by the letters P and S, are separated by about 5.5 sec.

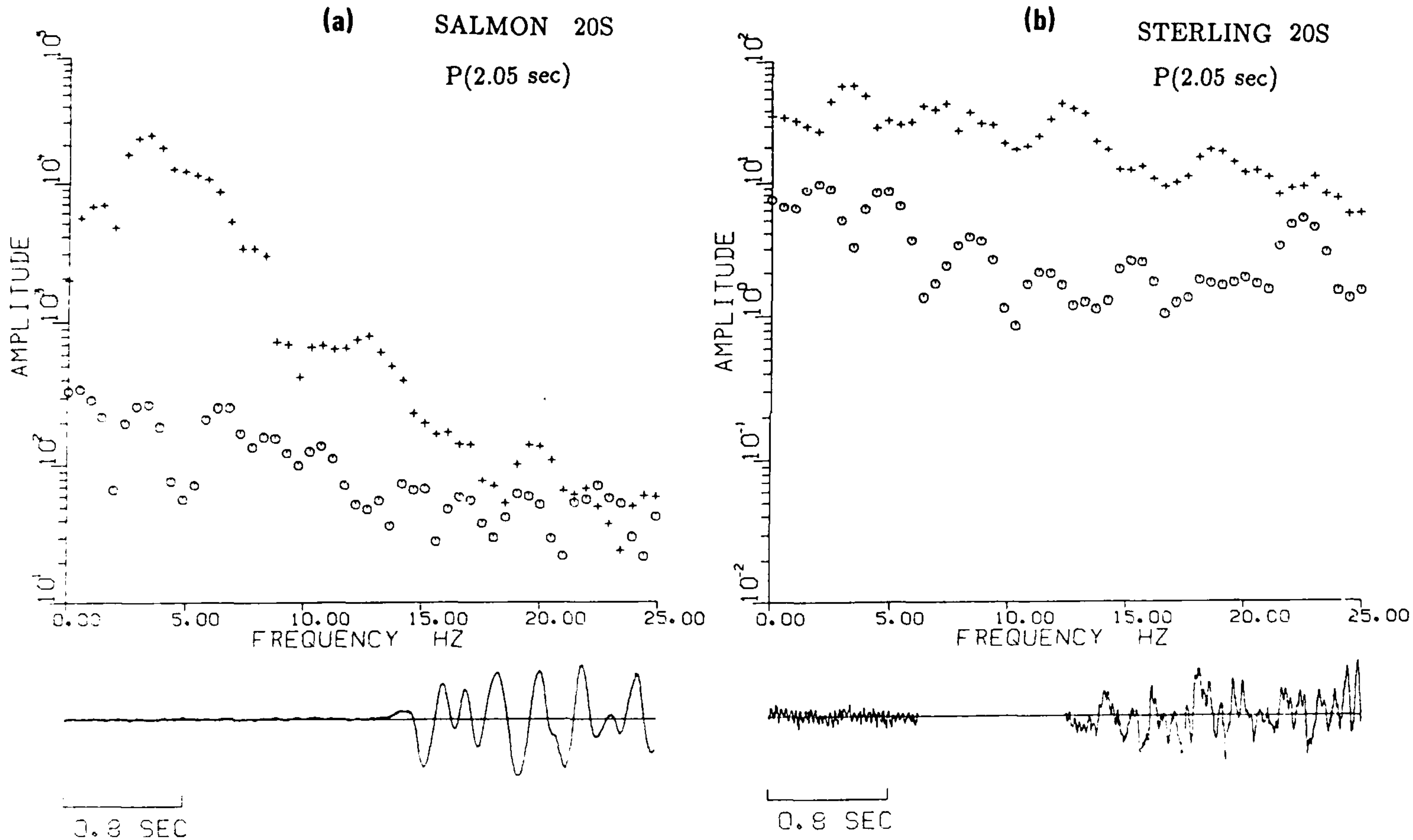

Figure 10. Spectra of the observed P arrivals (window 2.05 sec long) for (a) Salmon and (d) Sterling recorded at station 20S. The spectra of an equally long noise window prior to the onset of P are also shown. The amplitude values are in arbitrary units.

SALMON/STERLING 20S

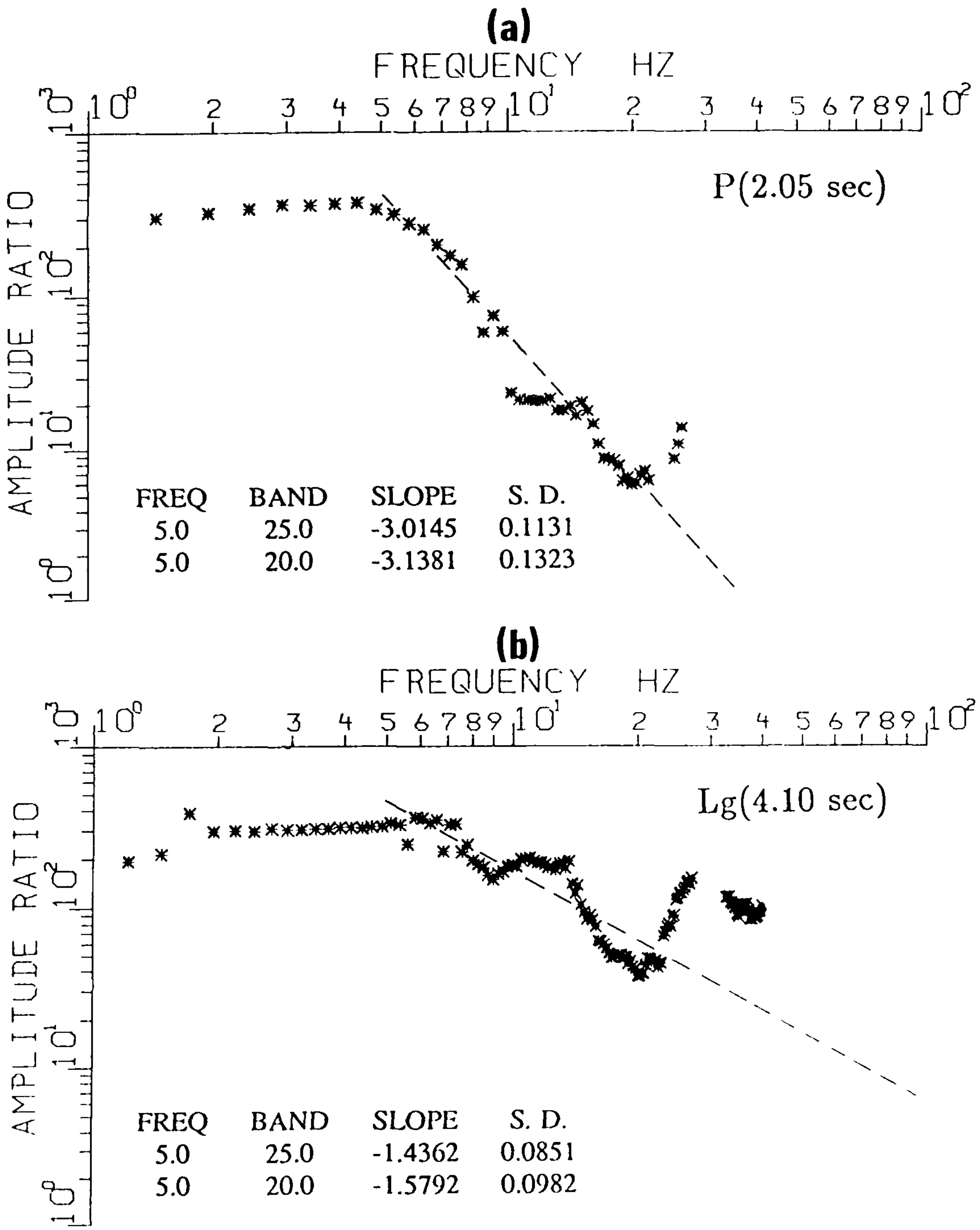

Figure 11. Spectral ratio Salmon/Sterling, corrected for noise, with logarithmic frequency scale, for (a) P window 2.05 sec long, and (b) Lg window 4.10 sec long, recorded at station 20S. The dashed lines show mean (least squares) slopes over the frequency range 5 to 25 Hz. The mean value of slope and its standard deviation (S.D.) are indicted for frequency ranges of 5 to 25 and 5 to 20 Hz.

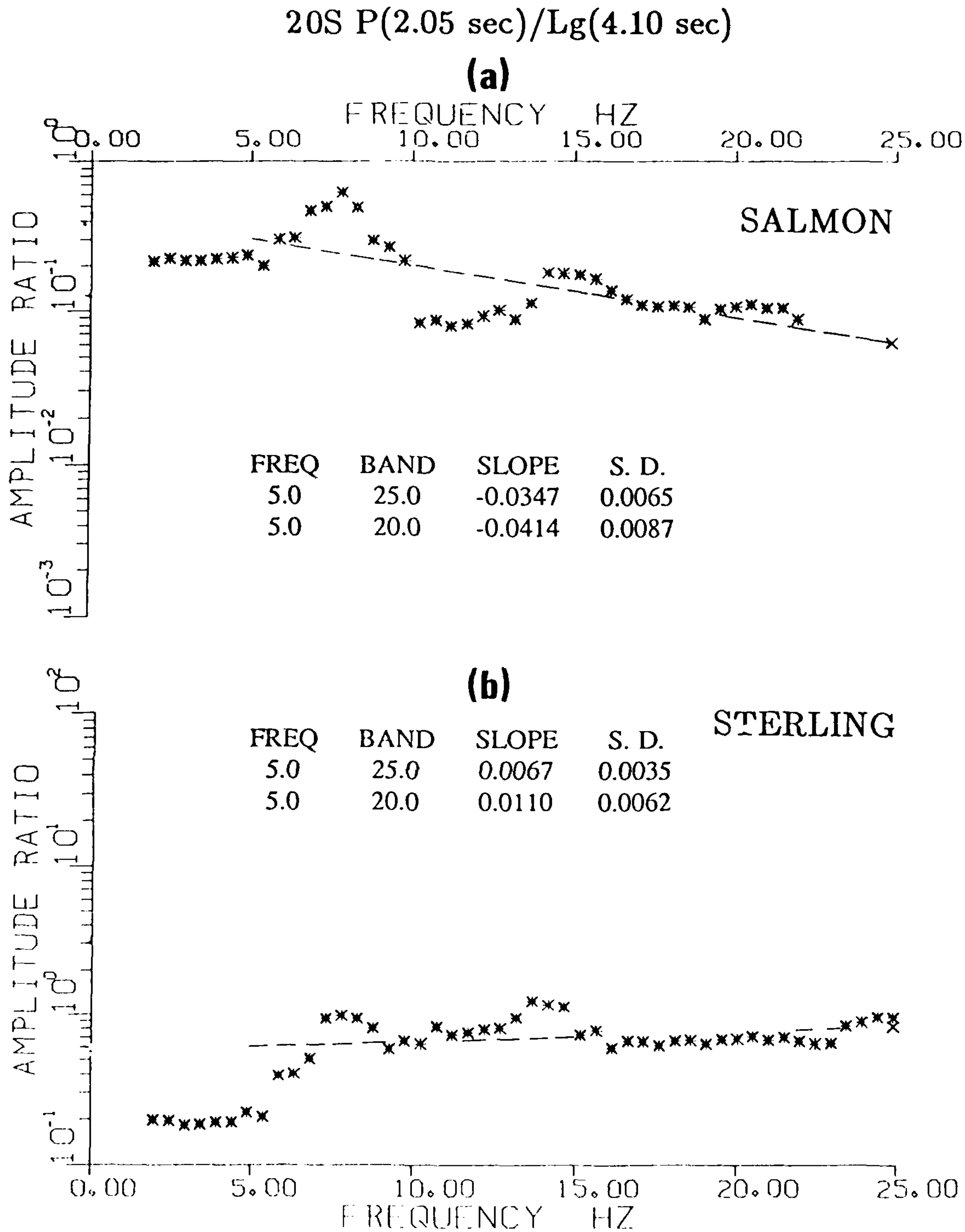

Figure 12. Spectral ratio P/Lg, corrected for noise, for (a) Salmon and (b) Sterling recorded at station 20S. Points for which S/N power ratio is less than 2 are not plotted. The dashed lines show mean (least squares) slopes over the frequency range 5 to 25 Hz. The mean value of slope/Hz and its standard deviation (S.D.) are indicted for frequency ranges of 5 to 25 Hz and 5 to 20 Hz.

ANALYSIS OF DATA FROM STATION PL-MS

We also analyzed the vertical component data for Salmon and Sterling recorded at the USGS station PL-MS, located 27 km south of ground-zero. The digitization rate for the PL-MS data was 100 samples/sec. The spectral ratios P/Lg for Salmon and Sterling, with the Lg window being 512 points (5.12 sec) long, are shown in Figure 13. The spectral modulations are again similar, especially for the lower frequencies. The values of mean slopes (dashed lines) are significantly smaller for Salmon than for Sterling. The difference between the two mean slope values is 0.0463 for the frequency range of 5 to 25 Hz, nearly equal to the difference observed at station 20S. These results are again similar to those obtained from data at stations 10S and 20S.

PL-MS P(2.56 sec)/Lg(5.12 sec)

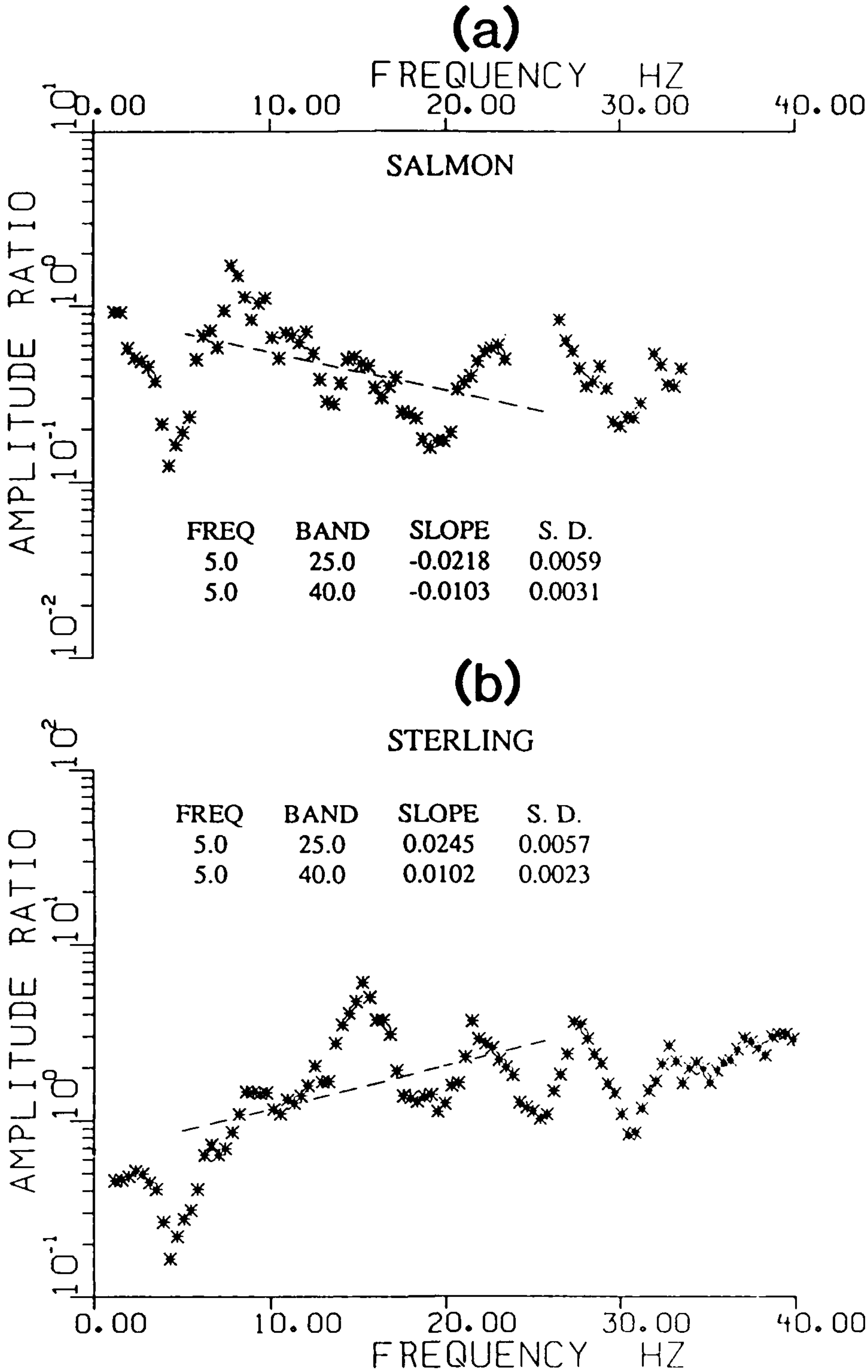

Figure 13. Spectral ratio P/Lg, corrected for noise, for (a) Salmon and (b) Sterling recorded at station PL-MS. Points for which S/N power ratio is less than 2 are not plotted. The dashed lines show mean (least squares) slopes over the frequency range 5 to 25 Hz. The mean value of slope/Hz and its standard deviation (S.D.) are indicated for frequency ranges of 5 to 25 and 5 to 40 Hz.

SPECTRAL ANALYSIS OF Pn AND Lg FROM NTS EXPLOSIONS

An examination of P and the Lg group data from the three stations 10S, 20S, and PL-MS, described above, shows exactly similar differences in the excitation of the two phases from Salmon and Sterling. An obvious major difference between Salmon and Sterling is in their scaled depths, defined as depth(m)/$W^{1/3}$ where W is yield in kt. In order to understand why the decoupling ratio is different for P and Lg, we therefore studied the spectral content of Pn and Lg from explosions covering a wide range of yields, shot depths, and scaled depths. For this purpose, we selected 7 Pahute Mesa (NTS) explosions, covering the yield range of 0.7 to 1100 kt (Table 1). Regional phases from these explosions were well recorded at the LRSM station, KN-UT (epicentral distance, $\Delta \approx 320$ km); Pn arrivals from these were studied by Blandford (1976). Two of the seven explosions, viz. Cabriolet and Schooner, were cratering shots. It is interesting to note that time-domain measurements of the amplitudes of regional phases (Pn, Pg, and Lg) from these 7 explosions failed to show any systematic differences between the shallowest (cratering) and the deepest and/or the most overburied explosions (Gupta et al., 1985).

TABLE 1

PAHUTE MESA AND SALT EXPLOSIONS USED IN SPECTRAL ANALYSES

No.	Name	Date	Shot Medium (m)	Shot Depth (m)	Depth of Water Table	Yield+ (kt)	Scaled Depth#
1	Buteo	12 May 65	tuff	696	660	0.7	784
2	Rex	24 Feb 66	tuff	671	642	16	266
3	Duryea	14 Apr 66	rhyolite	544	662	65	135
4	Scotch	23 May 67	tuff	977	672	150	184
5	Cabriolet*	26 Jan 68	rhyolite	52	488	2.3	39
6	Schooner*	8 Dec 68	tuff	111	274	35	34
7	Benham	19 Dec 68	tuff	1402	641	1100	136
8	Salmon	22 Oct 64	salt	828	-	5.3	475
9	Stercal	17 Nov 66	salt	831	-	0.0027	5968
10	Sterling	3 Dec 66	salt	829	-	0.38	1145

+ Values for NTS explosions from Springer and Kinnaman (1971) except for Buteo from an estimate, based on LR data, by Blandford (1976). Values for the three shots in salt from Springer et al. (1968).

* cratering explosion

depth(m)/$W^{1/3}$ where W is yield in kt.

Scaled depth is an important parameter directly influencing the spectra and amplitudes of explosion-generated body and surface waves (e.g. Rulev, 1965; and Kisslinger, 1963, for a review of early work). Table 1 lists the scaled depths not only for the 7 Pahute Mesa explosions but also for Salmon, Sterling, and Stercal. A large range of both shot and scaled depths are covered by these 10 explosions.

We obtained the spectral ratios of Pn/Lg on the vertical component records at the station, KN-UT for the seven Pahute Mesa (NTS) explosions listed in Table 1. To isolate the source effects, it is important to use as nearly common source-receiver paths as possible because of the extreme sensitivity to propagation paths of the regional phases, especially Lg (Gupta and Blandford, 1983). The seven explosions in Table 1 are all from Pahute Mesa so that the source-receiver paths to KN-UT should not be much different and the results should be nearly free from propagation path effects. The window lengths for Pn and Lg were 6.4 and 12.8 sec, respectively, and a 10% cosine taper was used along with 3 and 5 point smoothing of the spectra. Out of these 7 shots, Buteo and Duryea with their yields differing by a factor of about 100, were detonated in the same hole so that the source-receiver paths are almost identical. The spectra of Pn and noise windows for Duryea and Buteo are shown in Figure 14 which show good S/N up to about 7 Hz. The spectral ratios Duryea/Buteo for Pn and Lg windows, each corrected for noise, are shown in Figure 15. The fall-off with frequency rate is larger for the Pn ratio than for the Lg ratio, similar to the results for Salmon/Sterling in Figures 7 and 11. The spectral ratios Pn/Lg for Duryea and Buteo, corrected for noise, are shown in Figure 16 which indicates smaller spectral slope for Duryea than for Buteo, again similar to the Salmon and Sterling results of Figures 8, 12, and 13. Results from all 7 explosions (Table 1) are shown in Figure 17 in which the mean spectral slopes of Pn/Lg over the frequency range of 1 to 5 Hz are plotted versus the scaled depth (in log units). The plot indicates a linear trend with correlation coefficient of 0.810. This implies that the spectral ratio Pn/Lg is considerably influenced by scaled depth.

It is important to determine whether it is the spectra of Pn or Lg (or both) that vary strongly with scaled depth. A comparison of the spectral ratios for P or Pn and Lg, such as in Figures 7 and 11 for Salmon/Sterling and in Figure 15 for Duryea/Buteo, suggests that the Lg spectra are less variable or more stable than the P or Pn spectra. To explore this possibility on the observed data from the 7 Pahute Mesa explosions recorded at KN-UT, we compared the spectral content of the individual Pn and Lg windows after correcting for the large differences in the explosion yields. For the latter, we made use of von Seggern and Blandford's (1972) source scaling in which the source function for a given yield, W is expressed as

KN-UT Pn(6.4 sec)

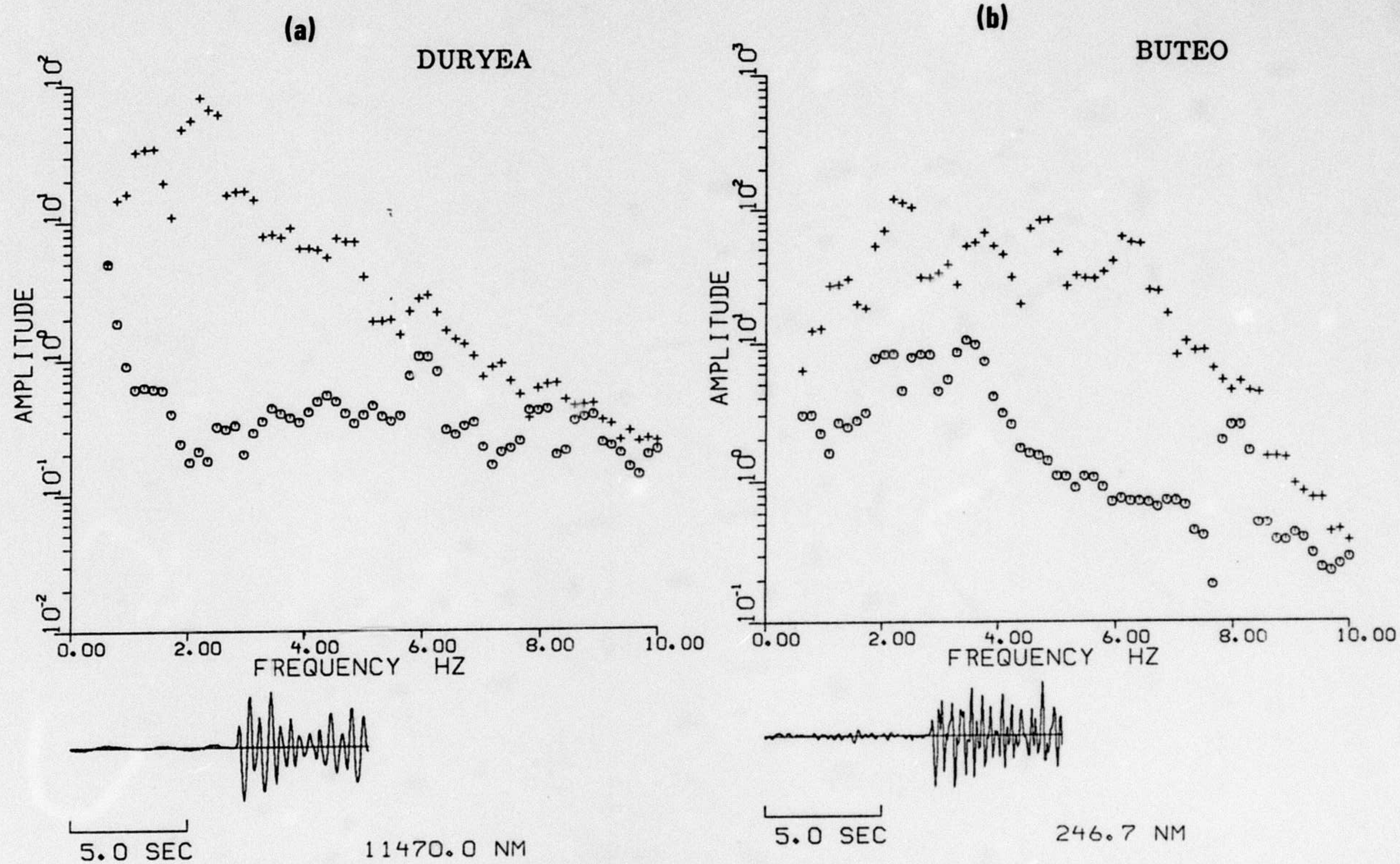

Figure 14. Spectra of the observed Pn arrivals (window 6.4 sec long) for (a) Duryea and (b) Buteo recorded at station KN-UT. The spectra of an equally long noise window prior to the onset of Pn are also shown. The peak amplitude values, noted under each trace, are in nanometers (nm).

KN-UT DURYEA/BUTEO

(a)

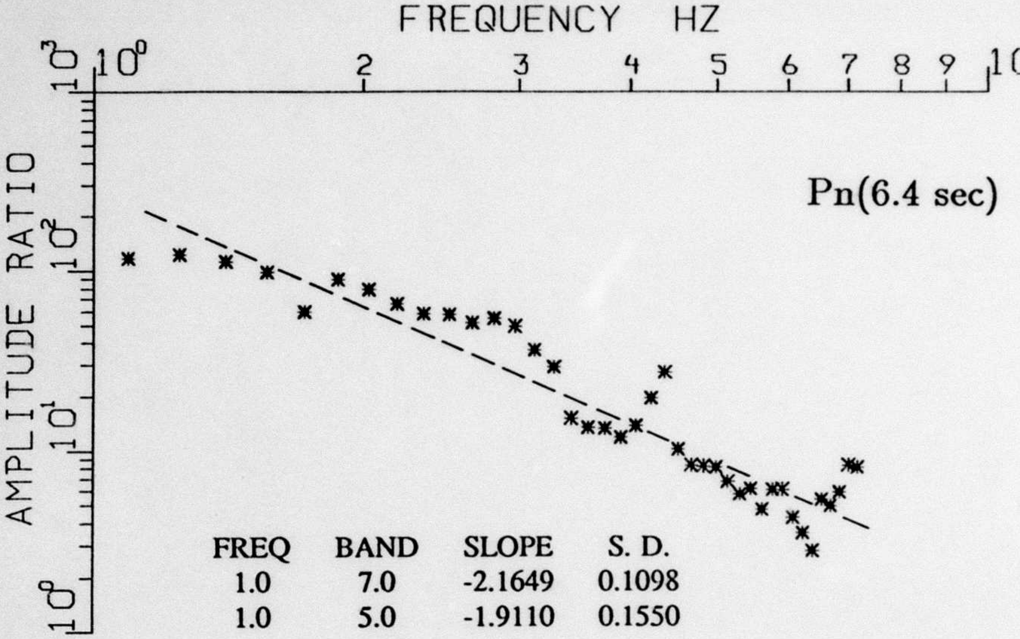

(b)

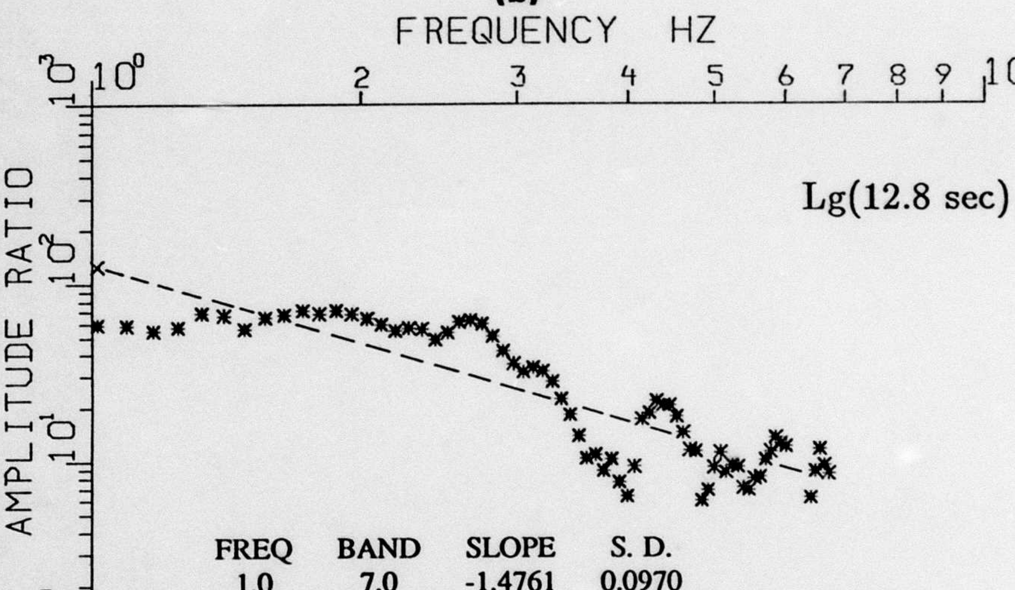

Figure 15. Spectral ratio Duryea/Buteo, corrected for noise, with logarithmic frequency scale, for (a) Pn window 6.4 sec long, and (b) Lg window 12.8 sec long. The dashed lines show mean (least squares) slopes over the frequency range 1 to 7 Hz. The mean value of slope/Hz and its standard deviation (S.D.) are indicated for frequency ranges of 1 to 7 and 1 to 5 Hz.

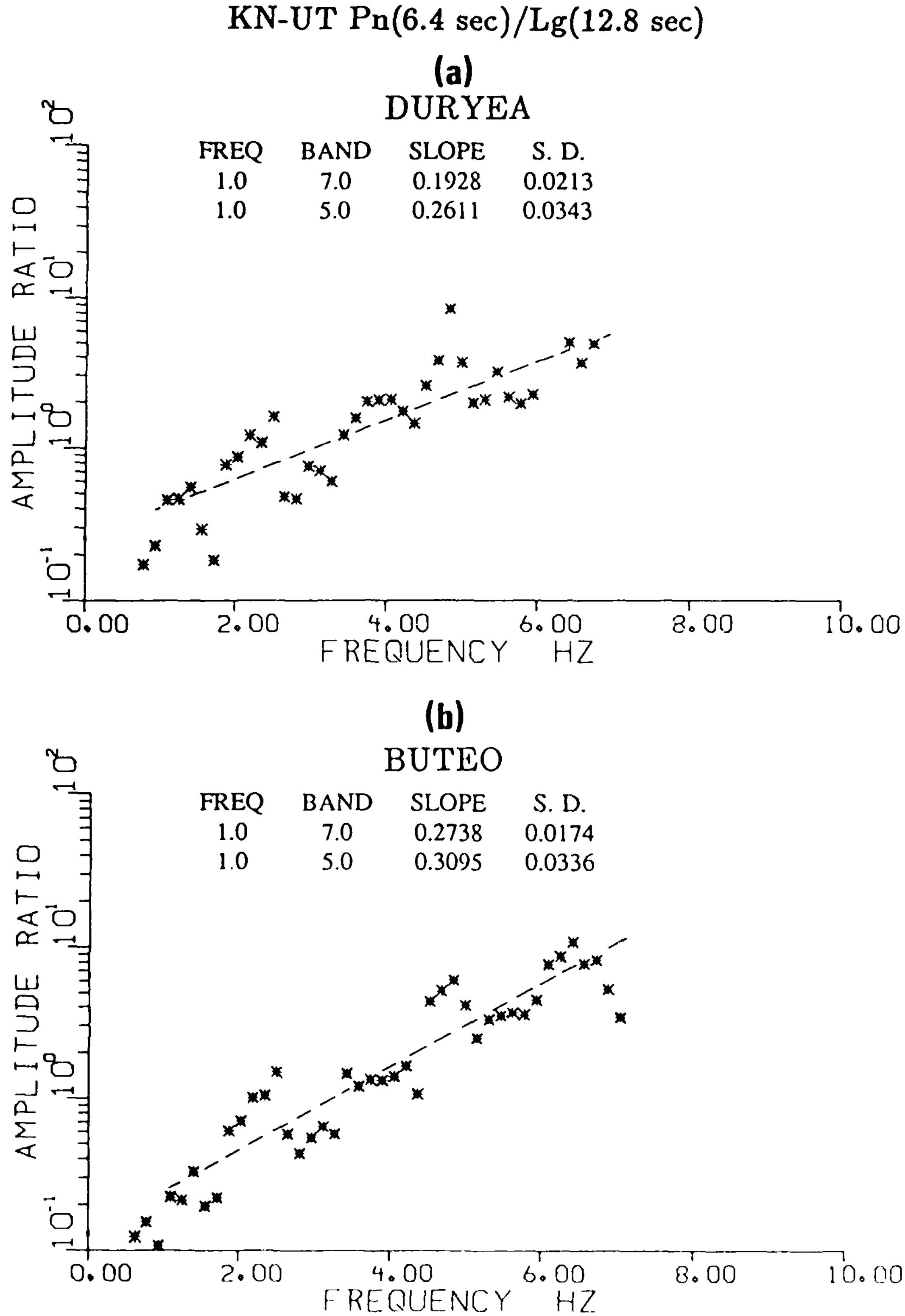

Figure 16. Spectral ratio Pn/Lg, corrected for noise, for (a) Duryea and (b) Buteo recorded at station KN-UT. Points for which S/N power ratio is less than 2 are not plotted. The dashed lines show mean (least squares) slopes over the frequency range 1 to 7 Hz. The mean value of slope/Hz and its standard deviation (S.D.) are indicated for frequency ranges of 1 to 7 Hz and 1 to 5 Hz.

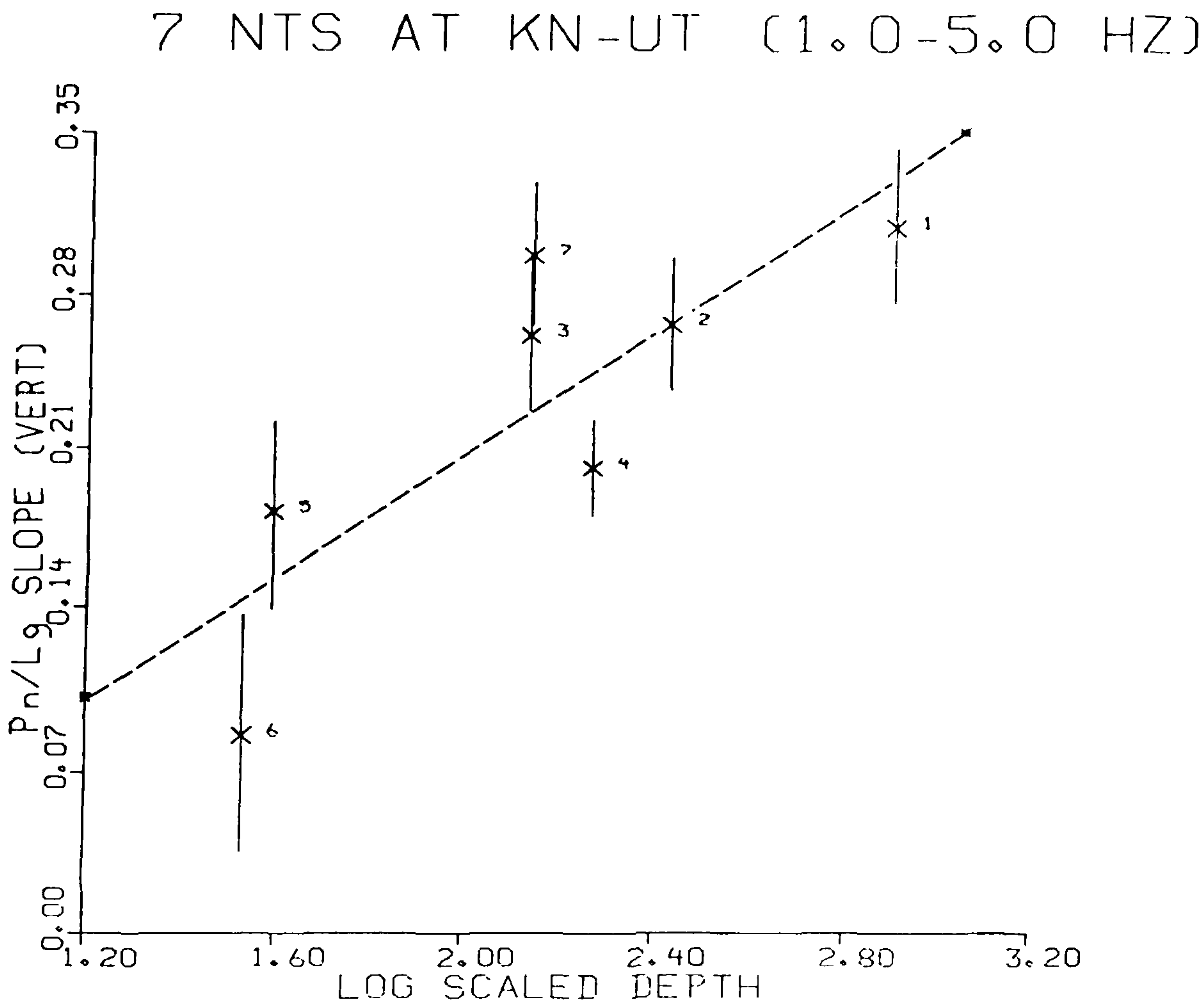

Figure 17. Mean Pn/Lg spectral slope (per Hz) over the frequency range 1 to 5 Hz versus log (scaled depth) for 7 explosions (numbered as in Table 1) recorded at station KN-UT. The least squares linear trend (dashed line) has a correlation coefficient of 0.810 and slope of 0.135. The vertical lines represent error bars with one standard deviation.

$$S(\omega) = W \frac{\left[A^2(\omega/k)^2 + 1\right]^{1/2}}{\left[(\omega/k)^2 + 1\right]^{3/2}} \Psi(\infty) \tag{1}$$

where $\omega = 2\pi f$, $\Psi(\infty)$ is a coupling term independent of frequency;

$$k = k_0 \, (5/W)^{1/3} \tag{2}$$

and

$$A = 2B + 1 \tag{3}$$

where B and k_0 are medium-dependent constants. In this model, shot depth is not an independent parameter but the source function can be varied by assigning different values to the rise time and overshoot parameters k_0 and B, respectively. Considering first the Pn windows for the various explosions, the spectra were corrected for the instrument response and anelastic attenuation by assuming $t^* = 0.1$, the value used by Blandford (1976). A correction for the differences in yields was applied by using the source function in equation (1) corresponding to a tuff reduced displacement potential (RDP), i.e. $k_0 = 12.0$ and $B = 0$. With these three corrections, the Pn spectra would become flat if the shot depth and medium did not influence the spectral shapes. Most of the corrected spectra were not flat and their mean spectral slopes indicated nearly linear trends; the results for Duryea and Buteo are shown in Figure 18. This means that ordinary cube-root scaling (i.e. with fixed values of parameters k_0 and B) fails to model the observed Pn spectra. A plot of the derived mean spectral slopes (such as those in Figure 18), over the frequency range 1.0 to 5.0 Hz, versus the scaled depth (in log units) is shown in Figure 19a. The least squares linear trend (dashed line) has correlation coefficient of 0.970 with mean slope of 0.206 indicating that, for a fixed yield, the Pn spectrum of an overburied (large scaled depth) explosion is richer in higher frequencies compared to that of an underburied (small scaled depth) explosion. This is in qualitative agreement with Mueller and Murphy's (1971) scaling in which scaled depth is not an important parameter but shot depth is relevant because of its influence on the overburden pressure. The same corrections (i.e. $t^* =$

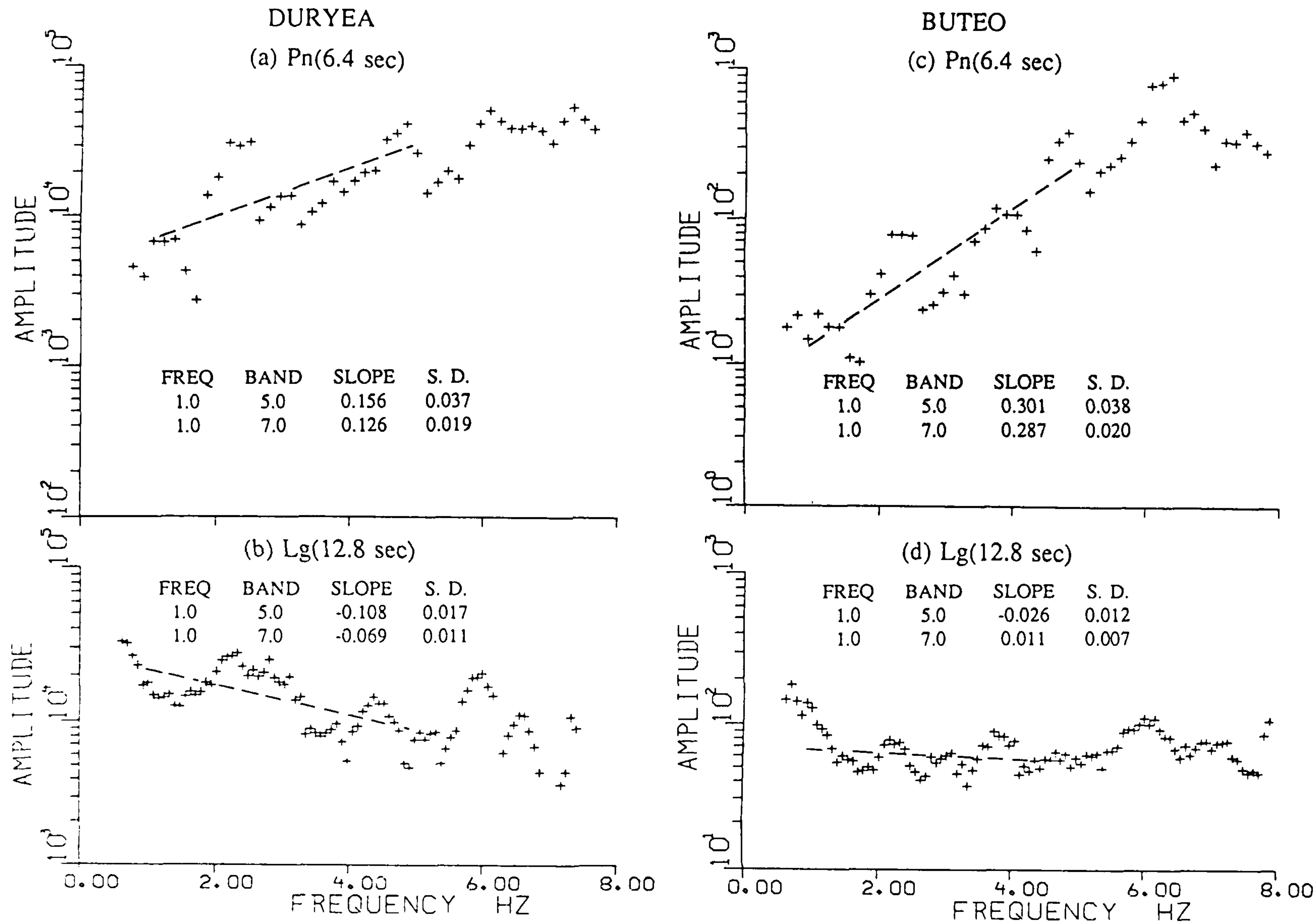

Figure 18. Spectra corrected for noise, source function, and t* for (a) Pn, (b) Lg, both from Duryea, (c) Pn, and (d) Lg, both from Buteo. The dashed lines show mean (least squares) spectral slopes over the frequency range 1 to 5 Hz. The mean value of slope/Hz and its standard deviation (S.D.) are indicated for frequency ranges of 1 to 5 Hz and 1 to 7 Hz.

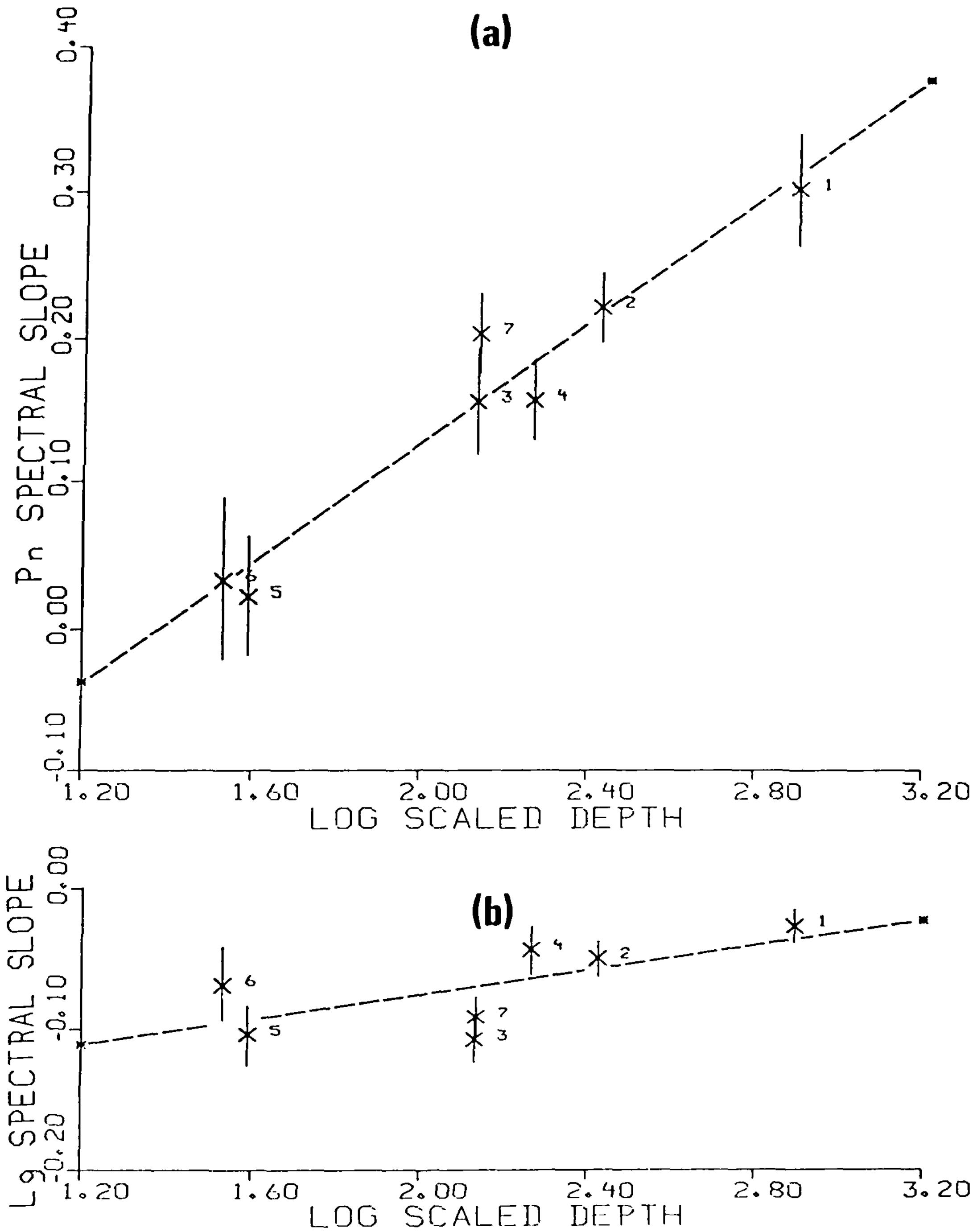

Figure 19. Mean spectral slope (per Hz) over the frequency range 1 to 5 Hz plotted versus log (scaled depth) for 7 explosions (numbered as in Table 1) recorded at station KN-UT for (a) Pn, the least squares linear trend (dashed line) has correlation coefficient of 0.970 and slope of 0.206; and (b) Lg, the least squares linear trend (dashed line) has correlation coefficient of 0.662 and slope of 0.045.

0.1 and tuff RDP) were also applied to the Lg spectra and the mean spectral slopes over the same frequency range computed. A plot of these slopes versus the scaled depth is shown in Figure 19b; the linear trend (dashed line) has correlation coefficient of 0.662 and mean slope of 0.045. Note that whereas the Pn slope values in Figure 19a cover a range of about 0.28 per Hz, the Lg slope values cover a range of only about 0.08 per Hz. This, together with the mean slope value for the data in Figure 19a being considerably larger than that in Figure 19b, suggest that, for a fixed yield, the Lg spectra (unlike the Pn spectra), are insensitive to variations in scaled depth.

Comparing results for the mean spectral slopes of Pn and Lg separately (Figures 19a and 19b) with those for Pn/Lg (Figure 17), it appears that most of the observed spectral differences between Pn and Lg are due to the spectra of P waves varying significantly with scaled depth whereas the spectra of Lg are insensitive to scaled depth. In other words, the observed variation in the spectral slope Pn/Lg is essentially due to the P-wave spectra being significantly more dependent on the scaled depth than the Lg spectra.

POSSIBLE EXPLANATION FOR VARIATION IN P/Lg FOR SALMON AND STERLING

At each of the three stations 10S, 20S, and PL-MS, the spectral ratio P/Lg was found to increase with increasing frequency, more positively for Sterling than for Salmon, i.e. the spectral slope was larger for larger scaled depth, in agreement with the results from 7 Pahute Mesa explosions recorded at KN-UT. Moreover, a comparison of the spectral ratios Salmon/Sterling for P and Lg suggested that the P spectra were considerably more variable (less stable) than the Lg spectra, again in agreement with the results from Pahute Mesa data. A possible explanation for the spectral ratio P/Lg to be different for P and Lg is therefore that the dependence on scaled depth of the P spectra is considerably larger than for the Lg group.

The scaled depths for Sterling and Salmon differ by a factor of 2.41 (see Table 1). If we assume that P/Lg ≈ Pn/Lg, then, on the basis of the empirical relationship in Figure 17, the mean spectral slopes P/Lg for the two explosions should differ by about 0.05/Hz. The observed differences from data at stations 10S, 20S, and PL-MS, over the frequency range of 5 to 25 Hz, are 0.015/Hz, 0.041/Hz, and 0.046/Hz, respectively (see Figures 8, 12, and 13). The agreement between expected and observed values is good for stations 20S and PL-MS but poor for station 10S, probably because the Lg group has not fully developed due to the small source-receiver distance. Note that Lg is the largest-amplitude phase for data at stations 20S and PL-MS but not at 10S.

A possible but not necessarily valid mechanism for the variability of Pn and stability of Lg spectra may be offered on the basis of RDP varying significantly with the takeoff angle, proposed earlier by Blandford (1976). The explosion cavity associated with an overburied shot is likely to be nearly spherical whereas that for a shot with smaller scaled depth is expected to approximate an ellipsoid with the long axis along the vertical direction. In terms of moment-tensor source (Aki and Richards, 1980, Chapter 3), a spherical cavity has $M_{11}=M_{22}=M_{33}$

whereas the equalities do not hold for non-spherical cavity. A source with azimuthal symmetry may have $M_{11} = M_{22} \neq M_{33}$ so that a cylindrically symmetric source extended in the vertical direction would appear, in the far field, to have the time function for M_{33} different than for M_{11} and M_{22}. For example, the corner frequencies and the DC levels of M_{11} and M_{22} would be higher than for M_{33} for a pressurized ellipsoid with major axis in the vertical direction (Glenn et al., 1986, especially their Figure 5).

Near-field subsurface data from nuclear explosions, sufficient to test the above possibility, perhaps do not exist. Limited data from Salmon, based on just two detectors, do appear to support the proposed mechanism, in spite of Salmon being an overburied shot with small expected source anisotropy. Figure 20a (after Figure 5.20, Perret, 1968) shows the measured RDP's based on the observed particle velocities at two detectors E6-27 and E14C-36, with takeoff angles, measured from the vertical, of 90 and 31 deg, respectively. The source-receiver distances are nearly equal so that the substantial difference in the two RDP's cannot be attributed to spatial attenuation. The initial pulse rises somewhat faster for the shot-level receiver, E6-27 than for the other receiver, E14C-36. Moreover, the static RDP value, which corresponds to the DC level in the far-field, is higher for E6-27 than for E14C-36. Similar results are obtained by analyzing the reduced velocity potential (RVP), which corresponds to the observed ground motion in the far-field. The RVP spectral ratio E6-27/E14C-36, based on signal windows of only about 0.2 sec each, is shown in Figure 20b. The effect of the free surface reflected phases (see Figure 10, Glenn et al., 1986) should be minimal since the signal windows are much smaller than the teleseismic pP - P time of about 0.58 sec. In Figure 20b, the source time function along the horizontal direction (E6-27) is richer in higher frequencies and has somewhat (about 3%) larger DC amplitude than that along the near-vertical direction (E14C-36), in qualitative agreement with Glenn et al. (1986).

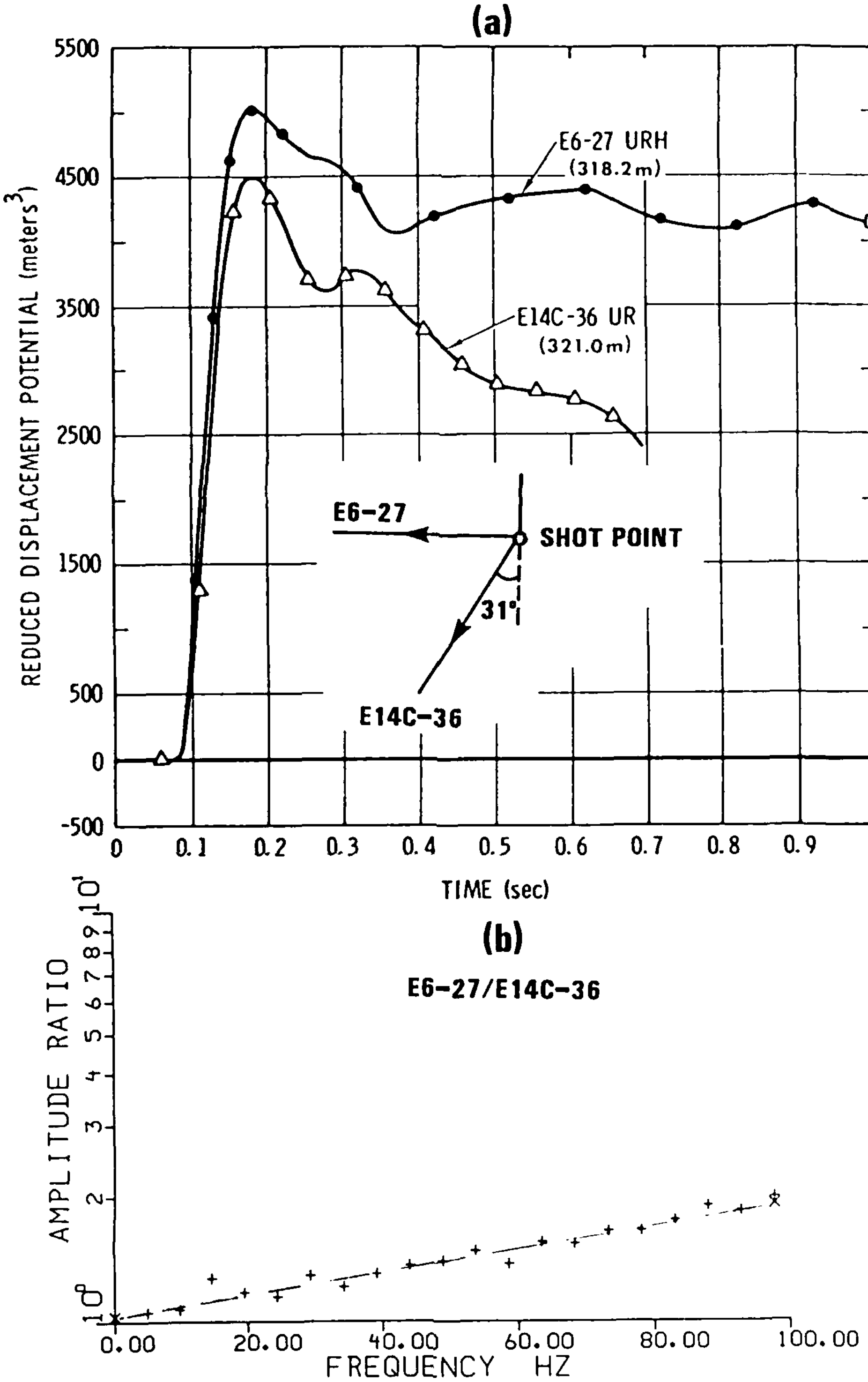

Figure 20. (a) RDP's derived from the observed radial horizontal particle velocity (URH) at E6-27 and radial particle velocity (UR) at E14C-36 with take-off angles of 90 and 31 degrees, respectively. Note the nearly equal shotpoint-to-receiver distances indicated for the two receivers. (b) RVP spectral ratio E6-27/E14C-36, corrected for noise and based on only about 0.2 sec of initial ground motion. The dashed line shows the mean (least squares) slope of 0.00273 per Hz (with standard deviation of 0.00014) over the frequency range of 1 to 100 Hz. The intercept value is 1.032.

Pn consists mainly of waves leaving the focal sphere at steep (nearly vertical) angles whereas Lg spans a large range of takeoff angles around the horizontal direction (see e.g. Campillo et al., 1985). Thus Pn is sensitive to variations in the M_{33} component whereas Lg is less sensitive to M_{33} because it averages over M_{11}, M_{22}, and M_{33}. For shots with small scaled depth, the effect of the source cavity will therefore be to shift the spectra of Pn to lower frequencies and that of Lg to relatively higher frequencies. Another contributing factor can be the non-linear free-surface effects, more intense for shots with smaller scaled depth and mostly confined to the region between the shot point and the free surface (e. g. Rimer et al., 1979, especially Figures 2.67 and 2.68). Vertically traveling waves that contribute directly to Pn, such as pP, will pass through this highly-fractured, large-strain, low-Q region and may become deficient in high frequencies. Frasier (1972) and Shumway and Blandford (1978) provided evidence that pP is deficient in higher frequencies as compared to direct P. Lg should be relatively free from these free-surface effects. We can thus qualitatively explain the observed increase in the Pn/Lg spectral slope with scaled depth such as that shown in Figure 17.

DISCUSSION AND CONCLUSIONS

A comparison of the P/Lg spectral ratios for Salmon and Sterling at stations 10S (Figure 8), 20S (Figure 12), and PL-MS (Figure 13) shows that most of the differences in the spectra of P and Lg lie in their high frequency contents. Similarly, for the NTS explosions recorded at KN-UT, the mean spectral slope of the spectral ratio Pn/Lg increases with scaled depth mostly because of differences in the Pn and Lg spectra at high frequencies (see Figure 16). In other words, the low frequencies in P and Lg are insensitive to variations in scaled depth whereas the high frequencies vary considerably with scaled depth. Flynn (1986) studied effects of source depth on near source seismograms by examining the spectra of P and SV-Rayleigh surface waves from five 115 kg chemical explosions buried at depths ranging from 1.8m (optimum cratering depth) to 11.5 m (fully contained). Energy in the high frequency band of 10 to 40 Hz, dominated by P waves, was found to increase significantly with source depth whereas energy in the low frequency band of 4 to 12 Hz, consisting mostly of SV-Rayleigh waves, was not a strong function of shot depth. Our results regarding the relative excitation of P and Lg are therefore in good agreement with those of Flynn (1986).

Underground nuclear explosions are generally very complex with both primary and secondary sources of seismic waves (e.g. Masse, 1981; Springer, 1974). Langston (1983) found a complex mechanism even for the decoupled shot Sterling. Blandford and Woolson (1979) noted evidence for possible azimuthal variation in the decoupling ratio for Salmon and Sterling. The idealization of an explosion source as a pressure pulse applied to the walls of a spherical cavity should perhaps be used to infer only qualitative results. Non-linear effects, known to be important for most nuclear explosions (especially those with shallower scaled depths), also drastically modify the seismic signals (Perl et al., 1979; Rimer et al., 1979; Day et al., 1985).

Analysis of data from Salmon, Sterling, and the Sterling Calibration shot recorded at both 10S and 20S indicate reduced decoupling at higher frequencies for both P and the Lg group. After correcting for the differences in yield of the three explosions, the reduction in decoupling for P is a factor of about 7 to 14 over the frequency range 1 to 20 Hz. The reduction in decoupling for Lg over the same frequency range is considerably smaller. Therefore, at high frequencies, Lg is more decoupled than P. These results are in agreement with the earlier work of Blandford and Woolson(1979). Note that the absolute calibration of data used in this study is somewhat uncertain so that the earlier estimates of the Salmon/Sterling decoupling ratio by Blandford and Woolson (1979) are to be preferred.

A comparison of the spectra of the direct P and the Lg group for Salmon and Sterling recorded at each of the three stations 10S, 20S, and PL-MS suggests the P-wave spectra to be significantly more variable than the Lg spectra. Analysis of Pn and Lg spectra from several Pahute Mesa shots recorded at a common station indicates similar results and a rather systematic dependence of the mean slope of the spectral ratio Pn/Lg on scaled depth. For a fixed yield, Pn spectra vary considerably with scaled depth whereas the Lg spectra are insensitive to scaled depth. Differences in the frequency dependence of decoupling for P and Lg are therefore probably due to the P spectra varying strongly with scaled depth and the Lg spectra being nearly independent of the scaled depth.

REFERENCES

Aki, K. and P. G. Richards (1980). *Quantitative Seismology,* W. H. Freeman and Company, San Francisco, California.

Blandford, R. R. (1976). Experimental determination of scaling laws for contained and cratering explosions, *SDAC-TR-76-3,* Teledyne Geotech, Alexandria, Virginia.

Blandford, R. R. and J. R. Woolson (1979). Experimental spectral analysis of Salmon/Sterling decoupling, *SDAC-TR-79-3,* Teledyne Geotech, Alexandria, Virginia.

Borcherdt, R. D., J. H. Healy, W. H. Jackson, and D. H. Warren (1967). Seismic measurements of explosions in the Tatum salt dome, Mississippi, *Tech. Letter Crustal Studies - 48,* U. S. Geological Survey.

Bouchon, M. (1982). The complete synthesis of seismic crustal phases at regional distances, *J. Geophys. Res. 87,* 1735-1741.

Campillo, M., J. Plantet, and M. Bouchon (1985). Frequency-dependent attenuation in the crust beneath central France from Lg waves: data analysis and numerical modeling, *Bull. Seism. Soc. Am. 75,* 1395-1411.

Day, S. M., N. Rimer, and T. G. Barker (1985). Numerical study of source depth effects on explosion magnitude, *DARPA/AFTAC Research Review Meeting, 2-3 December 1985,* Patrick Air Force Base, Florida.

Flynn, E. C. (1986). Effects of source depth on near source seismograms, *M. S. Thesis,* Southern Methodist University, Dallas, Texas.

Frasier, C. W. (1972). Observations of pP in the short-period phases of NTS explosions recorded at Norway, *Geophys. J. 31,* 99-109.

Glenn, L. A., B. Moran, A. J. C. Ladd, and K. A. Wilson (1986). Elastic radiation from explosively-loaded axisymmetric cavities, *Geophys. J. 86,* 119-136.

Gupta, I. N. and R. R. Blandford (1983). A mechanism for generation of short-period transverse motion from explosions, *Bull. Seism. Soc. Am. 73,* 571-591.

Gupta, I. N., K. L. McLaughlin, and R. A. Wagner (1985). Analysis of regional data from cratering and non-cratering nuclear explosions, *TGAL-85-5*, Teledyne Geotech, Alexandria, Virginia. 981-993.

Hannon, W. J. (1985). Seismic verification of a comprehensive test ban, *Science 227*, 251-257.

Kisslinger, C. (1963). The generation of the primary seismic signal by a contained explosion, *Vesiac State-of-the-Art Report 4410-48-X*, University of Michigan, Ann Arbor, Michigan.

Knopoff, L., F. Schwab, and E. Kausel (1973). Interpretation of Lg, *Geophys. J. 33*, 389-404.

Langston, C. A. (1983). Kinematic analysis of strong motion P and SV waves from the Sterling event, *J. Geophys. Res. 88*, 3486-3497.

Mueller, R. A. and J. R. Murphy (1971). Seismic characteristics of underground nuclear detonations, Part I. Seismic spectrum scaling, *Bull. Seism. Soc. Am. 61*, 1675-1692.

Perl, N., F. J. Thomas, J. Trulio, and W. L. Woodie (1979). Effect of burial depth on seismic signals, Vol. 1, *PSR Rept. 815*, Pacific Sierra Research Corp., Santa Monica, California.

Perret, W. R. (1968). Free-field particle motion from a nuclear explosion in salt, Part 1, *VUF-3012*, Sandia Laboratory, Albuquerque, New Mexico.

Rimer, N., J. T. Cherry, S. M. Day, T. C. Bache, J. R. Murphy, and A. Maewal (1979). Two-dimensional calculation of Piledriver, analytic continuation of finite difference source calculations, analysis of free field data from Merlin and summary of current research, *SSS-R-79-4121*, Systems, Science, and Software, La Jolla, California.

Rulev, B. G. (1965). The energy in a Rayleigh surface wave from explosions in different kinds of rock, *Izvestiya, Earth Physics Series*, 233-241.

Shumway, R. H. and R. R. Blandford (1978). On detecting and estimating multiple arrivals from underground nuclear explosions, *SDAC-TR-77-8*, Teledyne Geotech, Alexandria, Virginia.

Springer, D. L. (1974). Secondary sources of seismic waves from underground nuclear explosions, *Bull. Seism. Soc. Am. 64*, 581-594.

Springer, D., M. Denny, J. Healy, and W. Mickey (1968). The Sterling experiment: decoupling of seismic waves by a shot-generated cavity, *J. Geophys. Res. 73*, 5995-6011.

Springer, D. L. and R. L. Kinnaman (1971). Seismic source summary for U. S. underground nuclear explosions, 1961-1970, *Bull. Seism. Soc Am. 61*, 1073-1098.

Sykes, L. R. (1987). Underground nuclear explosions: verifying limits on underground testing, yield estimates, and public policy, *Rev. of Geophys. 25*, 1209-1214.

von Seggern, D. H. and R. R. Blandford (1972). Source time functions and spectra for underground nuclear explosions, *Geophys. J. 31*, 83-97.

Warren, D. H., J. H. Healy, and W. H. Jackson (1966). Crustal seismic measurements in southern Missouri, *J. Geophys. Res. 71*, 3437-3458.

(THIS PAGE INTENTIONALLY LEFT BLANK)

SECTION B

STRAIN AND FREQUENCY DEPENDENT ATTENUATION ESTIMATES IN SALT FROM SALMON AND STERLING NEAR-FIELD RECORDINGS

SUMMARY

The amplitude and spectra of teleseismic and regional seismic P waves depend on the material properties in the source region. The effects of strain and frequency dependent attenuation are therefore important for understanding the source characteristics of coupled versus decoupled explosions. Near-field velocity and acceleration data from the Salmon and Sterling explosions in salt were analyzed for strain and frequency dependent attenuation. Attenuation, parameterized as 1/Q, was estimated for various source-receiver distance ranges and frequency bandwidths by using two methods: (a) mean spectral ratio slope and (b) average amplitude spectral ratio. Results from Salmon indicate that (1) in the frequency range of 1-25 Hz, Q is about 5 to 10; (2) Q increases with source-receiver distance, suggesting lower Q for larger strain levels; (3) Q in the frequency range of 25-50 Hz is substantially higher than in the frequency range of 1-25 Hz, or Q increases with frequency. Analysis of data from Sterling indicates that Q is frequency independent and about one order of magnitude larger than for Salmon. Therefore the near-source attenuation was strain and frequency dependent and hence non-linear for Salmon out to a range of 600 m.

LIST OF FIGURES

INTRODUCTION

It is important to understand the attenuation and other characteristics of rocks in the vicinity of an explosive source because of their direct impact on far-field amplitudes and spectra. The detection of explosions and the discrimination of explosions from earthquakes depends on these far-field P wave spectra, therefore in the context of verification the importance of understanding tamped and decoupled explosions in salt becomes critical (Hannon, 1985; Evernden et al., 1986). In this study, we have analyzed subsurface strong-motion data from the Salmon explosion in salt and the decoupled shot, Sterling, detonated in the cavity created by Salmon. Both of these nuclear explosions were recorded by a large array of subsurface strong motion accelerometers and velocity gauges (Perret 1968a, b). These data are useful for determining source differences between the tamped explosion, Salmon and the decoupled shot, Sterling, because most of the receivers remained at the same locations for both explosions. The shot-point to receiver range covered by these subsurface instruments was from 166 m to 740 m, or scaled distances between 95 m/kt$^{1/3}$ to 427 m/kt$^{1/3}$. The regional P wave corner frequency of Salmon suggests an equivalent elastic radius, a, between 240-290 m (Larson, 1979). Data collected from a variety of shots in salt (the Cowboy series of chemical explosions, Salmon, and Sterling) indicate that inelastic effects extend to a scaled radius of 3.6 m/kg$^{1/3}$ (velocities of 0.5 m/sec, strains of 10^{-4}, and a $\simeq$ 600 m for Salmon), and that anelastic attenuation continues to at least 30 m/kg$^{-1/3}$ (Minster and Day, 1986). Workman and Trulio (1985) present evidence from the Cowboy Trails experiments that the inelastic effects in salt extend to 11.3 km/kt$^{-1/3}$. The decoupled explosion, Sterling, was shot in the Salmon cavity (radius $\simeq$ 17 m, Springer et al., 1968) and the subsurface measurements lie nearly within the linear region. It would seem therefore that the subsurface measurements for Salmon and Sterling were made at distances which may span the transition from non-linear inelastic into linear anelastic response of the salt.

NEAR-FIELD DATA FROM SALMON AND STERLING

A detailed description of the subsurface and surface strong-motion data from Salmon is given by Perret (1968a). The azimuthal relationship of each instrument boring to ground zero (designated Station 1A) and the range and angular elevation between each instrument station and the working point are shown in Figure 1 (after Figure 2.2, Perret, 1968a).

The strong-motion data from Salmon indicate peak radial particle velocity to attenuate with source-receiver distance, r as $r^{-1.9}$ and the peak strains (peak velocity/ propagation velocity) vary from about $4x10^{-3}$ to $3x10^{-4}$ (Perret, 1968a, especially Figure 5.11). The Sterling data indicate peak radial particle velocity to attenuate approximately as r^{-1} and the peak strains span the range of about $3x10^{-5}$ to about $7x10^{-6}$ (Perret, 1968b, especially Figure 3.6). The Salmon data have significant signal content from 1 to over 200 Hz whereas most of the Sterling data are usable to 400 Hz. Records of all horizontal and vertical digitized velocity gauge data from Salmon are shown in Figure 2 (the 12 instrument stations are designated as A, B, C, D, E, F, G, H, J, K, L, and M). The numbers near the observed waveforms indicate zero-to-peak velocity m/sec. The particle motion is up for radial motion away from the source or for upward vertical motion. Stations C, H, K, and M have depths nearly equal to the shot depth so that vertical data from these 4 stations represent transverse motion. Similar available data from Sterling are shown in Figure 3.

Since the natural frequencies and/or damping factors of the recording instruments varied from one location to another, all available accelerometer and velocity gauge data were first corrected for the instrumental response and velocity records were derived. Before comparisons between various receiver locations could be made, it was found necessary to correct the particle velocity values for frequency-dependent near-field geometrical spreading. Reduced Velocity Potentials (RVP's) were estimated from both radial and vertical (whenever not transverse to the

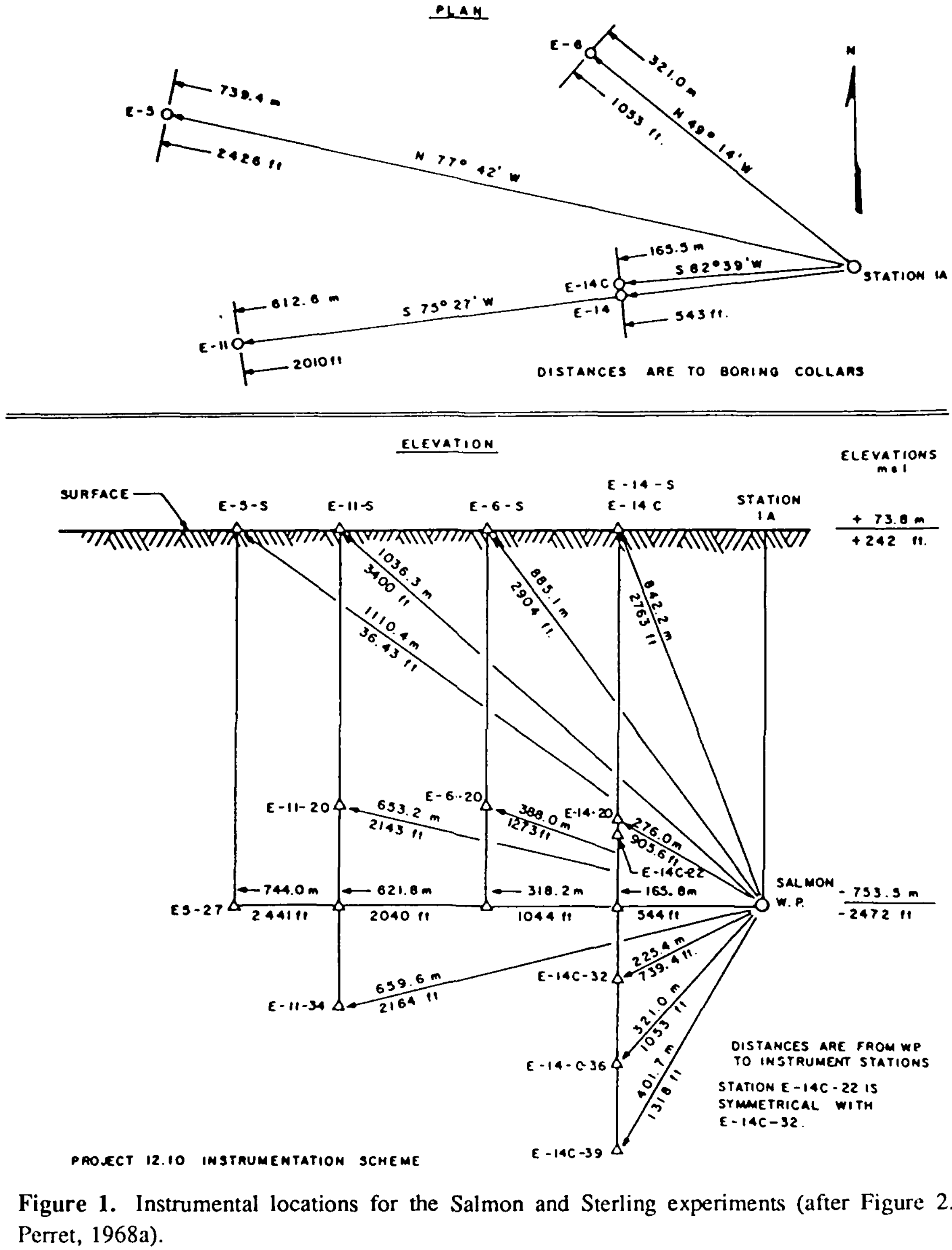

Figure 1. Instrumental locations for the Salmon and Sterling experiments (after Figure 2.2, Perret, 1968a).

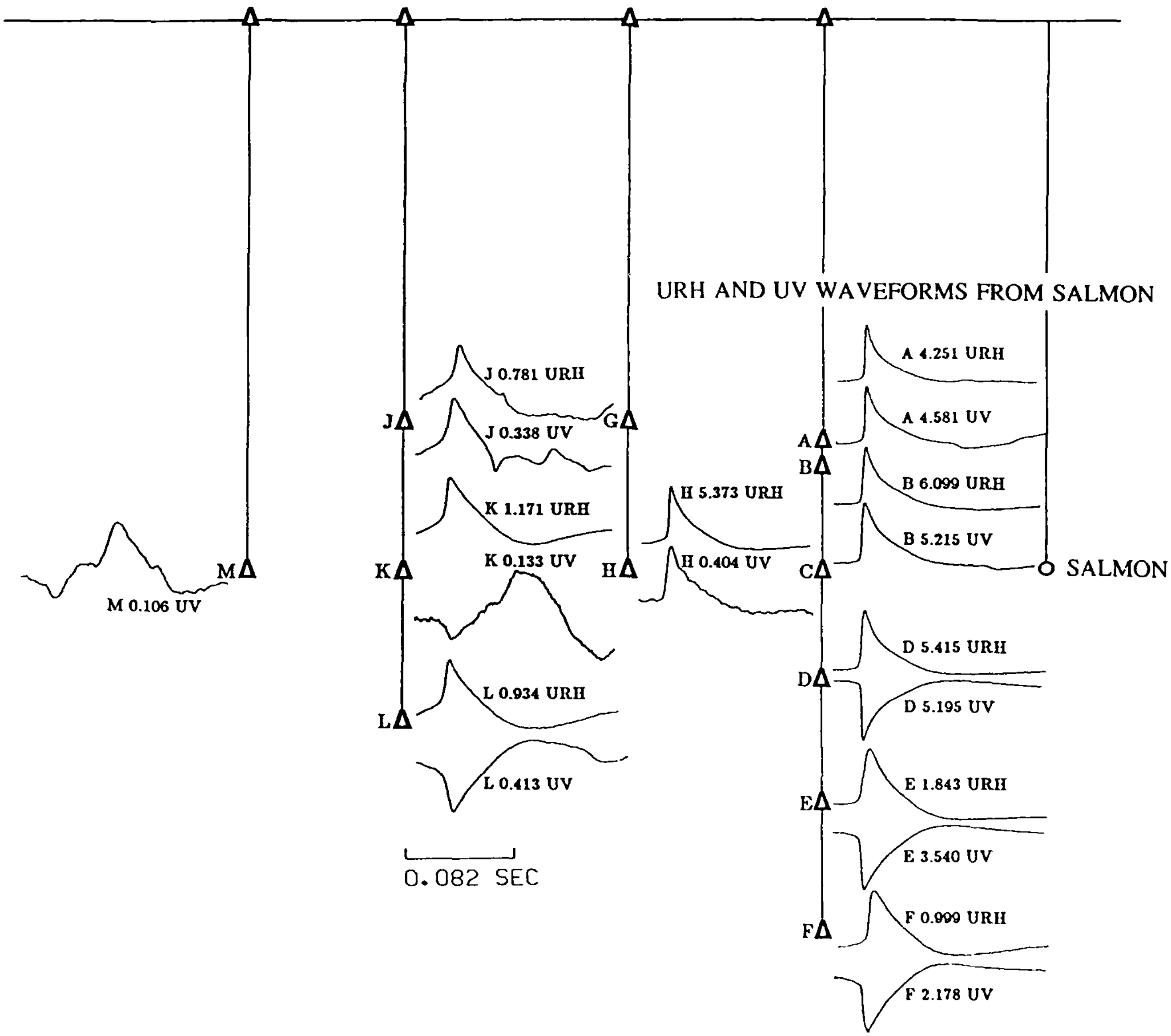

Figure 2. Particle velocity records from Salmon. URH indicates horizontal velocity, UV vertical velocity. Numbers indicate peak velocity in m/sec. Letters A through M indicate the gauge locations used in the analysis.

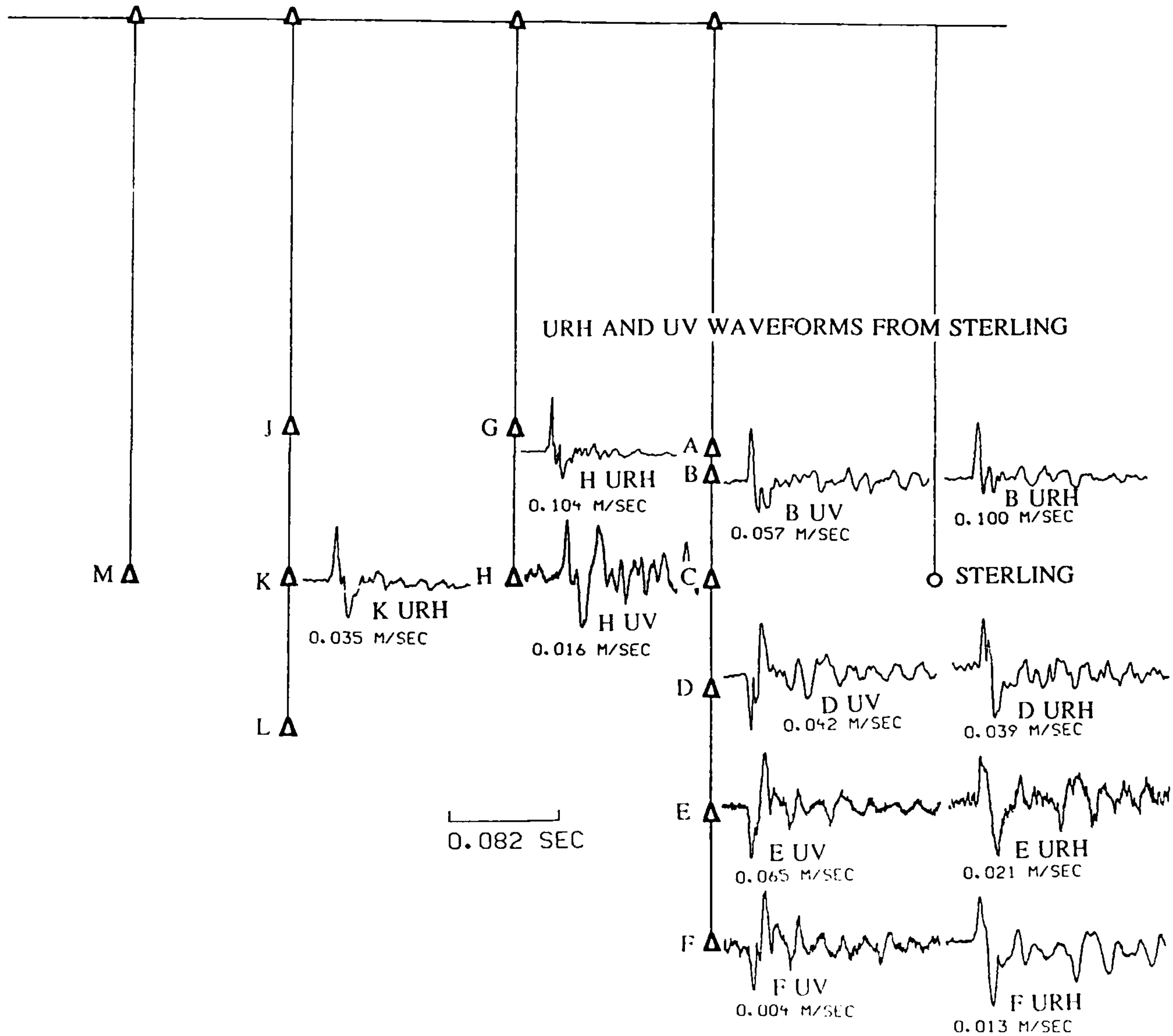

Figure 3. Similar to Figure 2 for Sterling.

source-receiver direction) component data from subsurface velocity gauges and accelerometers.

ESTIMATION OF NEAR FIELD ATTENUATION

Although the distances investigated here are admittedly within the non-linear regime, we have chosen to quantify the attenuation of the equivalent far-field P-wave source (RVP) with the familiar parameterization 1/Q. Therefore, we assume that at least incrementally, the spectrum of the compressional pulse attenuates as $\exp(\frac{-\pi fr}{Qc})$. $\frac{dA(f,r)}{dr} \approx \frac{-\pi f}{Qc} A(f,r)$ is therefore a quasilinear approximation for the non-geometric attenuation of the waveform spectra. However, in this case we consider the possibility that attenuation is dependent on strain level (therefore distance r) and frequency, $Q = Q(f, r)$. Work along these lines has been reported by Minster and Day (1986) and McCartor and Wortman (1985). Minster and Day (1986) argued that the peak velocity data from the series of experimental chemical explosives detonated in salt show that the attenuation must be both frequency and strain dependent. McCartor and Wortman (1985) examined the Salmon data and concluded that the attenuation of the RVP must be frequency dependent. Previously, it was noted that a frequency independent $Q \approx 10$ would account for the observed decay of Salmon peak velocities with distance like $r^{-1.9}$ rather than r^{-1} expected from simple geometrical spreading.

Our approach has been to extend the analysis of 1/Q(f) measured from the Salmon data to as many sensors available and to investigate the strain dependence, 1/Q(f, r), by examining the distance ranges available. In order to stabilize the estimation of the attenuation, we have estimated 1/Q for specific frequency bands; 1-25, 25-50, 50-100, 100-200, and 1-200 Hz. These attenuation estimates were made in two ways; 1) a spectral slope was estimated and 2) the average spectral ratio level was estimated for each pair of sensors and each frequency band. These measurements are essentially $\overline{t^*}$ and t^* estimates from the spectral slope and spectral level measurements, respectively. The two estimates are related for a frequency dependent attenuation by the familiar relation, $\overline{t^*} = t^* + f\frac{dt^*}{df}$ (e.g. Der et al., 1982). For our problem at hand, the 1/Q measured between two different sensors becomes the average 1/Q(r) between two distance ranges, r_i, and r_j. The attenuation estimated from the spectral slope of the spectral ratio between sensors i and j is designated $\overline{1/Q_{ij}}(f)$, while the attenuation derived from the average spectral level is $1/Q_{ij}(f)$. The two are related by, $\overline{1/Q_{ij}(f)} = 1/Q_{ij}(f) + f\,\frac{d(1/Q_{ij}(f))}{df}$, where we assume that $1/Q_{ij}(f) = \frac{1}{r_j - r_i}\int_{r_i}^{r_j}\frac{dr}{Q(f,r)}$ and similarly, $\overline{1/Q_{ij}}(f) = \frac{1}{r_j - r_i}\int_{r_i}^{r_j}\frac{dr}{\overline{Q(f,r)}}$.

Typical RVP spectra for Salmon and Sterling are shown in Figure 4. Note the scalloping of the Sterling spectra due to the added complexities of detonation in a cavity, such as pressure spikes (Larson, 1979). Typical RVP spectral ratios are shown in Figures 5A, 5B, 5C for Salmon. Note the curvature of the plotted spectral ratios. It is not possible to produce such a spectral ratio without an increase in Q with increasing frequency. This is the same basic measurement used by McCartor and Wortman to estimate frequency dependent Q(f) for the Salmon data. If we compare the spectral ratios from Salmon to those of Sterling in Figures 5C and 5D, we see that although the Sterling data is modulated by spectral scalloping, the average $\overline{Q}$ derived from Salmon cannot accommodate the data from Sterling. The average $\overline{Q}$ from the Sterling data in the 1 to 200 Hz bandwidth is 200 while the average Salmon $\overline{Q}$ derived from both spectral slopes and absolute spectral levels is less than 40. These average $\overline{1/Q}$ estimates are distinct at the three σ confidence level (see Table 1). Previous estimates of the near-field Sterling attenuation were $Q_S \approx 35$ and $Q_P \approx 70$ by Langston (1983) who modeled the rise times of P and S acceleration waveforms as a function of distance in the salt.

The $1/Q_{ij}$ and $\overline{1/Q_{ij}}$ estimates and their estimated uncertainties were tabulated for the 1-25, 25-50, 50-100, 100-200, and 1-200 Hz bandwidths. The estimates for the 1-25 and 1-200 Hz bands can be seen in Figures 6A, 6B, and 6C where the horizontal bars represent the distance range over which the attenuation estimates were made. Weighted averages over all sensor

(a) SALMON

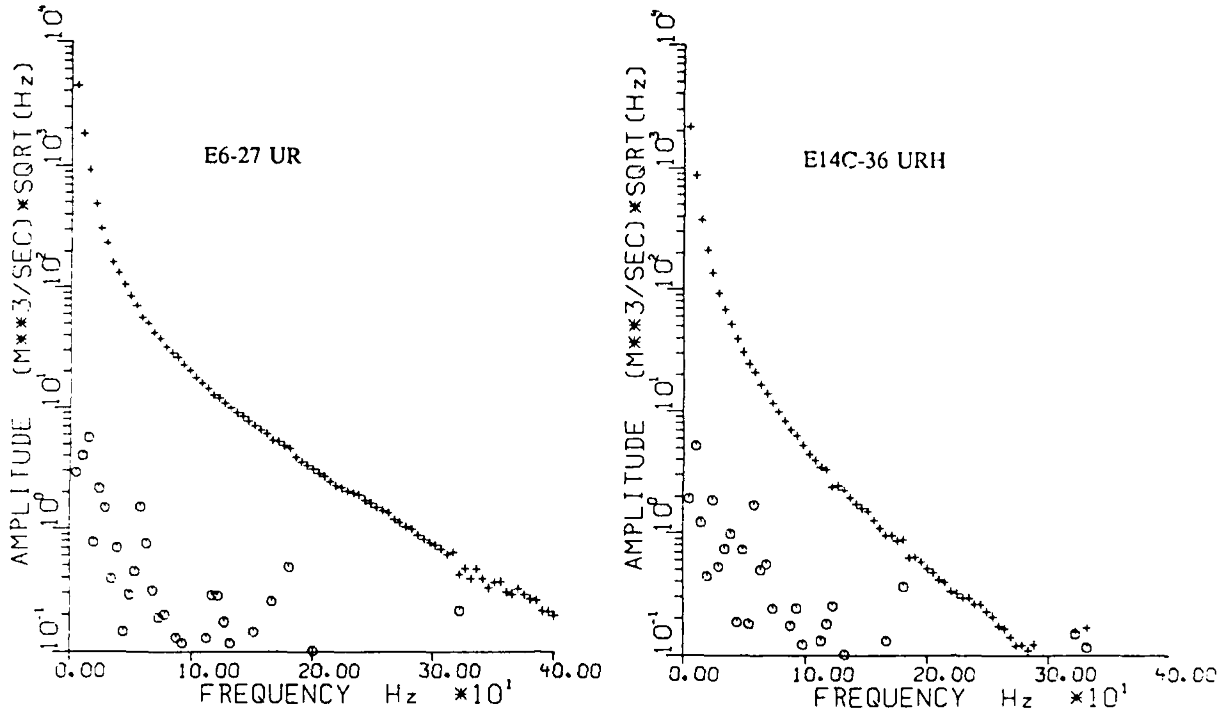

(b) STERLING

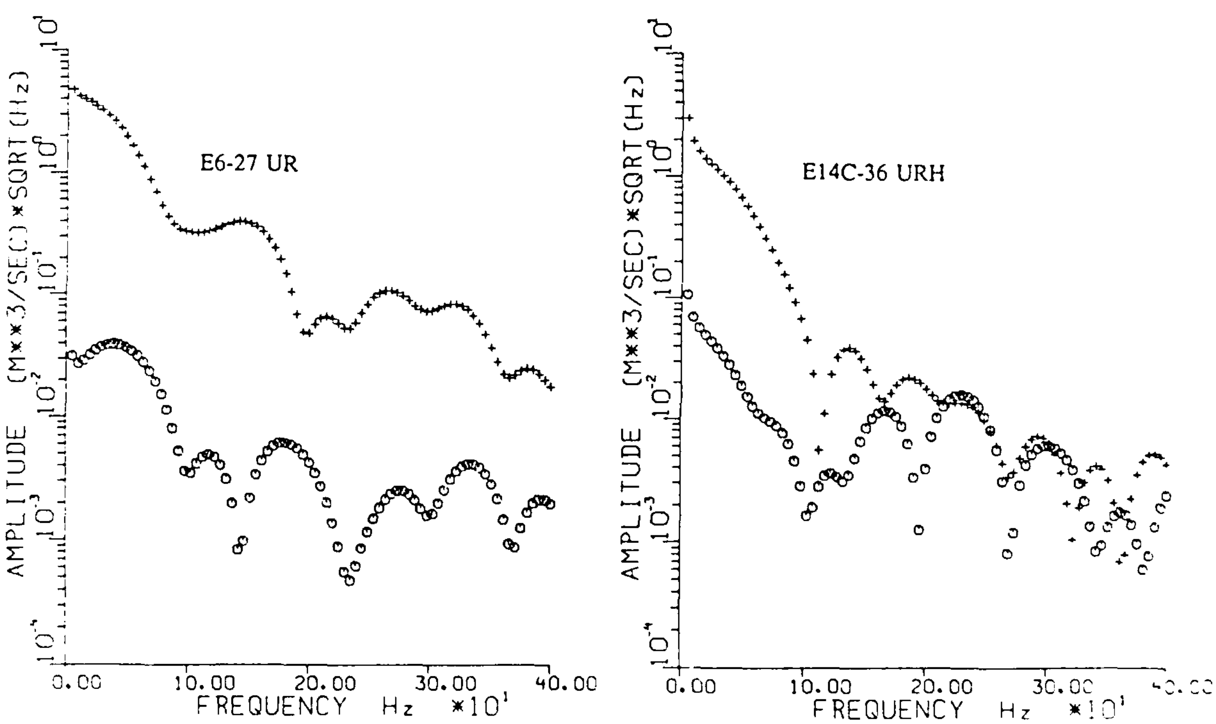

Figure 4. Spectra of RVP obtained from particle velocity data from Salmon and Sterling at nearly equidistant locations E6-27 (r = 318.2 m) and E14C-36 (r = 321.0 m)

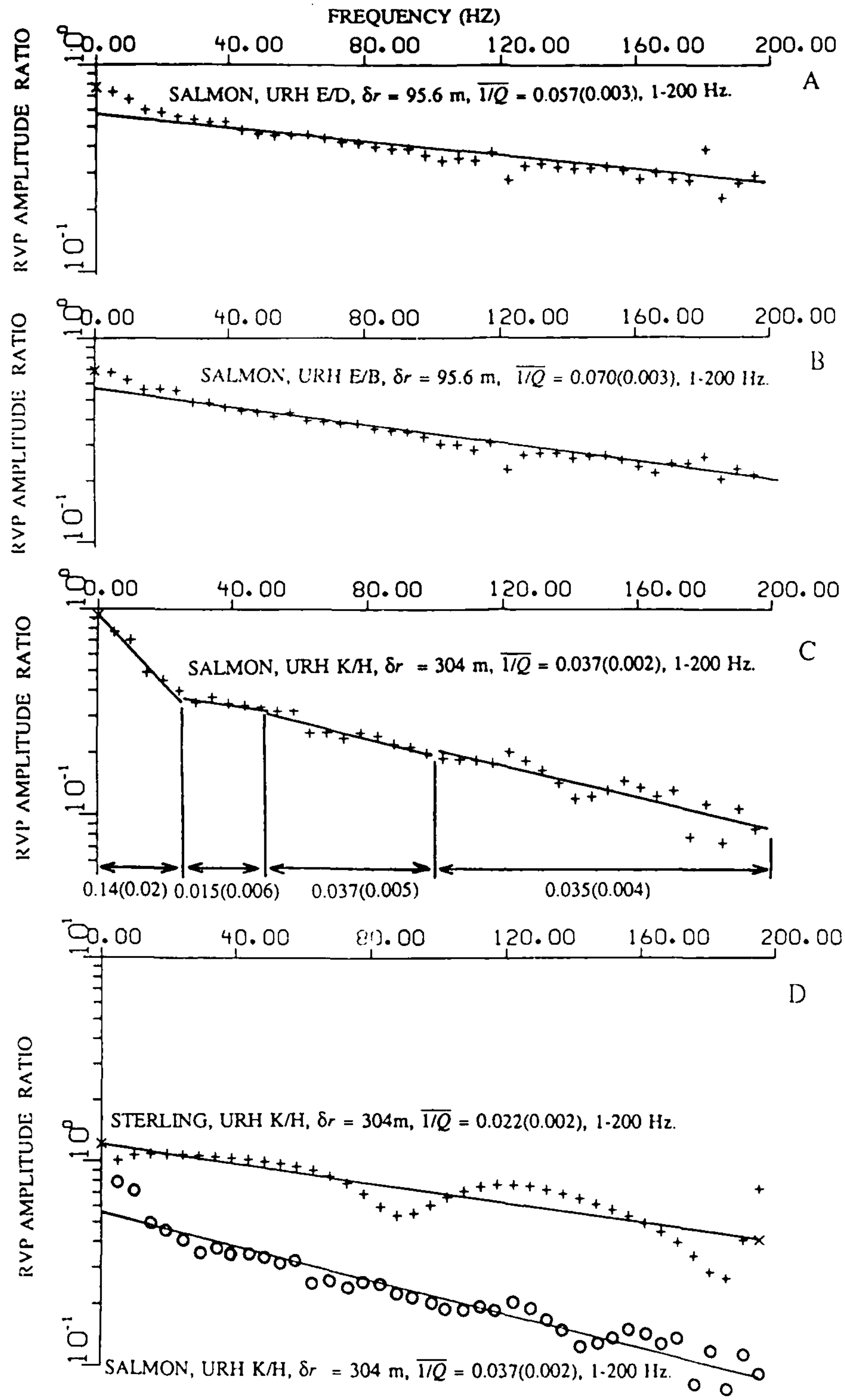

Figure 5. RVP spectral ratios of (5A) Salmon sensors E/D, (5B) Salmon E/B, (5C) Salmon sensors K/H, and (5D) Sterling sensors K/H (pluses) and Salmon sensors K/H (circles). Note the curvature of the Salmon spectral ratios E/D, E/B and K/H indicating the increase of Q with increasing frequency. The $\overline{1/Q}$ values for Salmon K/H are indicated for the 1-25, 25-50, 50-100, and 100-200 Hz frequency bands. Note the difference in the K/H spectral ratio for common sensors pairs for Salmon and Sterling.

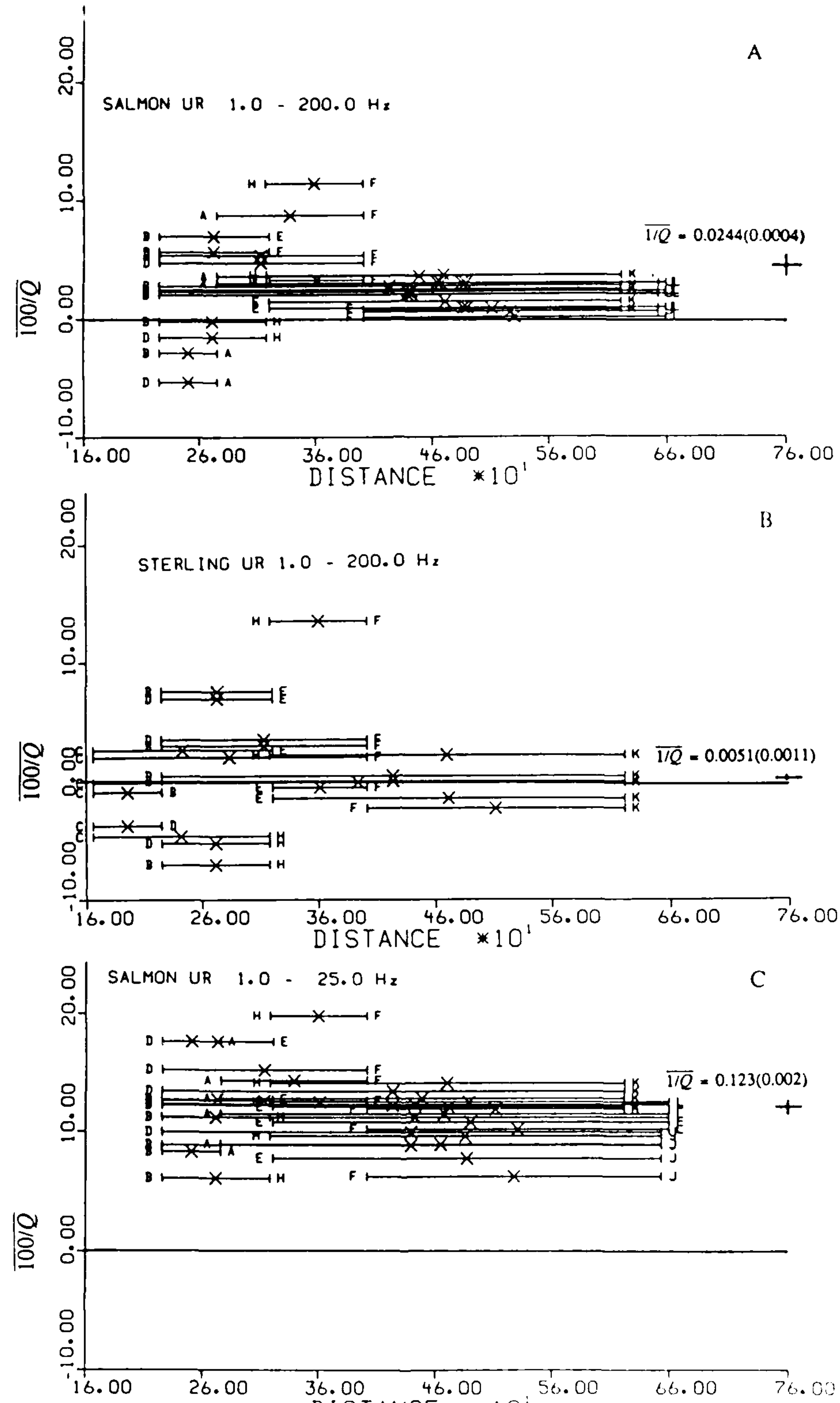

Figure 6. (6A) $\overline{1/Q}$ estimates for Salmon in the 1-200 Hz bandwidth from the URH sensor pairs. Mean $\overline{1/Q}$ = 0.0244(0.0004), or $\overline{Q}$ = 40.9(0.7). (6B) $\overline{1/Q}$ estimates for *Sterling* in the 1-200 Hz bandwidth from the URH sensor pairs. Mean $1/Q$ = 0.0051(0.0011) or $\overline{Q}$ = 196(40). (6C) $\overline{1/Q}$ estimates for Salmon in the 1-25 Hz bandwidth from the URH sensor pairs. Mean $\overline{1/Q}$ = 0.123(0.002), or $\overline{Q}$ = 8.1(0.1).

combinations are presented in Tables 2 and 3. The average attenuation estimates from the horizontal velocity (URH), vertical velocity (UV), horizontal acceleration (ARH), and vertical acceleration (AV) sensors are listed separately as well as all sensors together (ALL) in Tables 2 and 3. Q(f) must substantially increase with increasing frequency for Salmon between the 1-25 and 100-200 Hz bands.

TABLE 1. COMPARISON OF $\overline{1/Q}$ FOR SALMON AND STERLING

	SALMON					STERLING				
FREQ BAND	$\overline{1/Q}$	σ	Q	σ	n	$\overline{1/Q}$	σ	Q	σ	n
1-25	0.1235	0.0014	8.1	0.1	99	0.0026	0.0002	389	37	87
1-200	0.0290	0.0002	34.5	0.3	99	0.0026	0.0005	384	71	87

TABLE 2. MEAN 1/Q ESTIMATES FOR SALMON

FREQ BAND	ALL	AV	ARH	UV	URH
1-25	0.16(0.08)	0.21(0.02)	0.09(0.04)	0.14(0.02)	0.15(0.01)
25-50	0.096(0.006)	013(0.01)	0.09(0.01)	0.09(0.01)	0.10(0.01)
50-100	0.059(0.004)	0.073(0.007)	0.056(0.004)	0.055(0.004)	0.059(0.007)
100-200	0.049(0.003)	0.051(0.003)	0.0042(0.003)	0.037(0.003)	0.040(0.006)
1-200	0.049(0.003)	0.061(0.004)	0.0047(0.005)	0.044(0.003)	0.0047(0.007)

TABLE 3. MEAN $\overline{1/Q}$ ESTIMATES FOR SALMON

FREQ BAND	ALL	AV	ARH	UV	URH
1-25	0.09(0.01)	0.18(0.04)	0.04(0.02)	0.11(0.02)	0.119(0.006)
25-50	0.009(0.008)	0.07(0.02)	-0.02(0.01)	0.01(0.02)	0.01(0.01)
50-100	0.026(0.002)	0.019(0.003)	0.026(0.002)	0.15(0.007)	0.026(0.008)
100-200	0.026(0.002)	0.034(0.005)	0.026(0.002)	0.025(0.0004)	0.016(0.005)
1-200	0.029(0.002)	0.033(0.003)	0.032(0.002)	0.025(0.004)	0.026(0.006)

The $\overline{1/Q_{ij}}$ data were inverted for distance dependence, 1/Q(r), by a weighted least squares procedure. The average $\overline{1/Q}$ was determined for each distance range bracketed by the sensor distances. The results are shown in Figure 7 for 1-25 Hz. The Salmon 1-25 Hz near-field

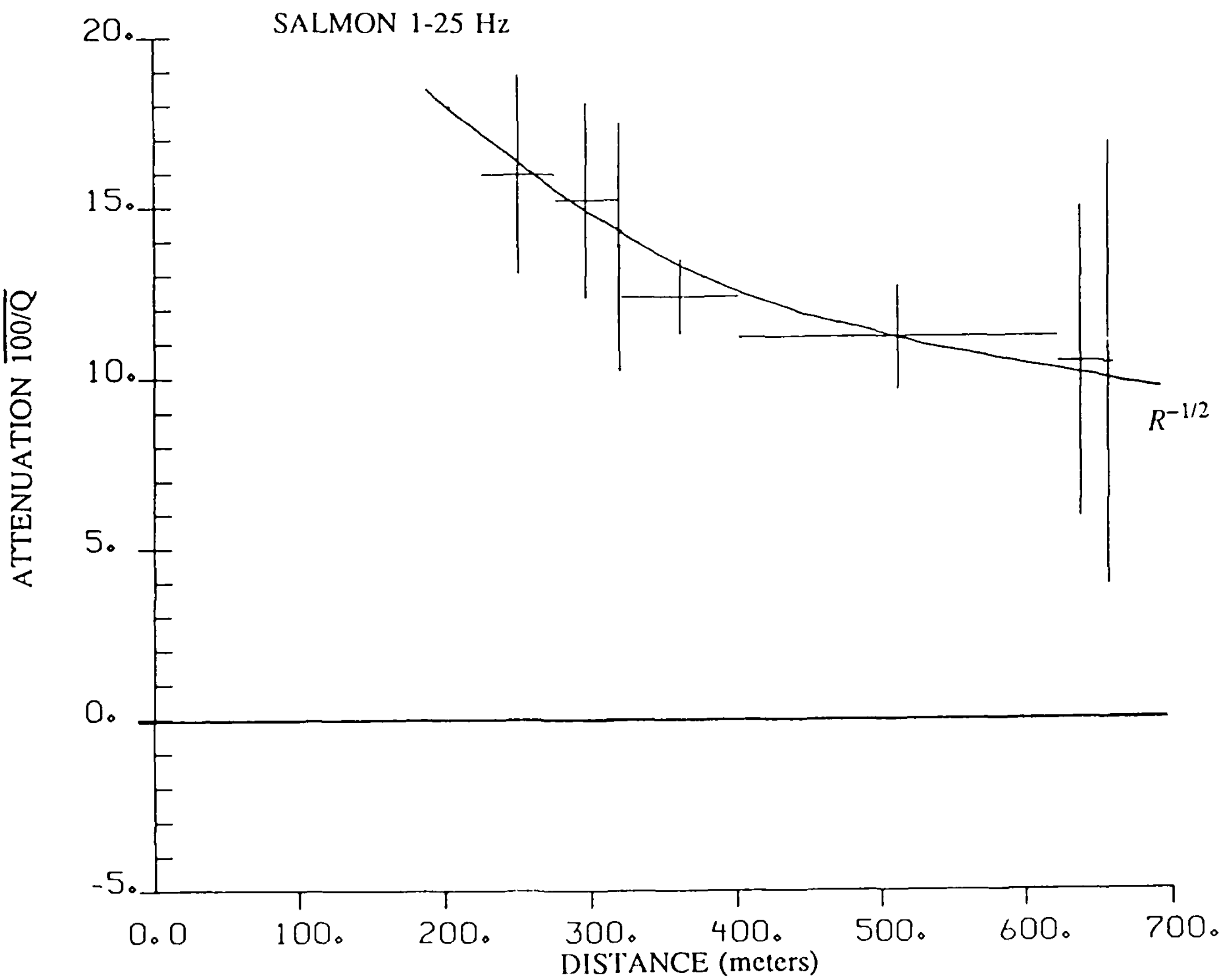

Figure 7. A weighted least squares fit of the 1-25 Hz Salmon RVP spectral ratio attenuation estimates for a fit against distance. $\overline{1/Q}$ is consistent with a $R^{-1/2}$ decay with distance.

attenuation declines by nearly 50% between 200 and 600 meters. Because the attenuation is smaller for the higher frequencies, it is less certain that there exists a distance dependence in the rate of attenuation for the 25-200 Hz range.

The 1 to 25 Hz $\overline{1/Q(r)}$ appears to decline like $r^{-1/2}$ rather than like $r^{-1.9}$ as would be expected if the attenuation rate were proportional to the strain level, ε. The near-field attenuation of the Sterling RVP was so little that no reliable distance dependence can be seen over such a short distance. Therefore it may be possible to consider the Sterling Q as the low strain-rate background Q level for salt. It is interesting that McCartor and Wortman (1985, see appendix A) have shown that the peak velocity data for explosions in salt could be consistent with attenuation proportional to $\sqrt{\varepsilon}$ or to ε^2, as well as directly proportional to ε. Since the Minster and Day model was derived from data at strains less than the Salmon data it is not clear whether a transition from $\varepsilon^{1/2}$ to ε occurs near strains of 10^{-4} or whether another parameterization of the Cowboy data is possible.

The data require that the attenuation rate be frequency dependent as well as depend upon the strain level. The net difference between the average 1/Q and the $\overline{1/Q}$ in the 1-25 Hz range is consistent with an average slope of 1/Q(f) of -0.002 Hz^{-1} in the 1-25 Hz bandwidth. This is also consistent with the net average difference between the average 1/Q and $\overline{1/Q}$ between 1-25 and 25-50 Hz bandwidths; -0.002 Hz^{-1}. These data are summarized in Table 4 for each frequency band. Assuming that 1/Q, $\overline{1/Q}$ and $(\overline{1/Q}-1/Q)/f$ are smooth functions of frequency, we can derive a model that accommodates both the absolute spectral ratio levels as well as the average slopes of the spectral ratios. This 1/Q(f) model is plotted in Figure 8. The model differs from McCartor and Wortman's model where they parameterize their model as $1/Q(f) = \gamma_0 + \gamma_1 f^{-1}$. $f\frac{d(1/Q)}{df}$ = a constant for the McCartor and Wortman parametrization. We find that this parameterization is inconsistent with the data of Tables 2 and 3. The changing curva-

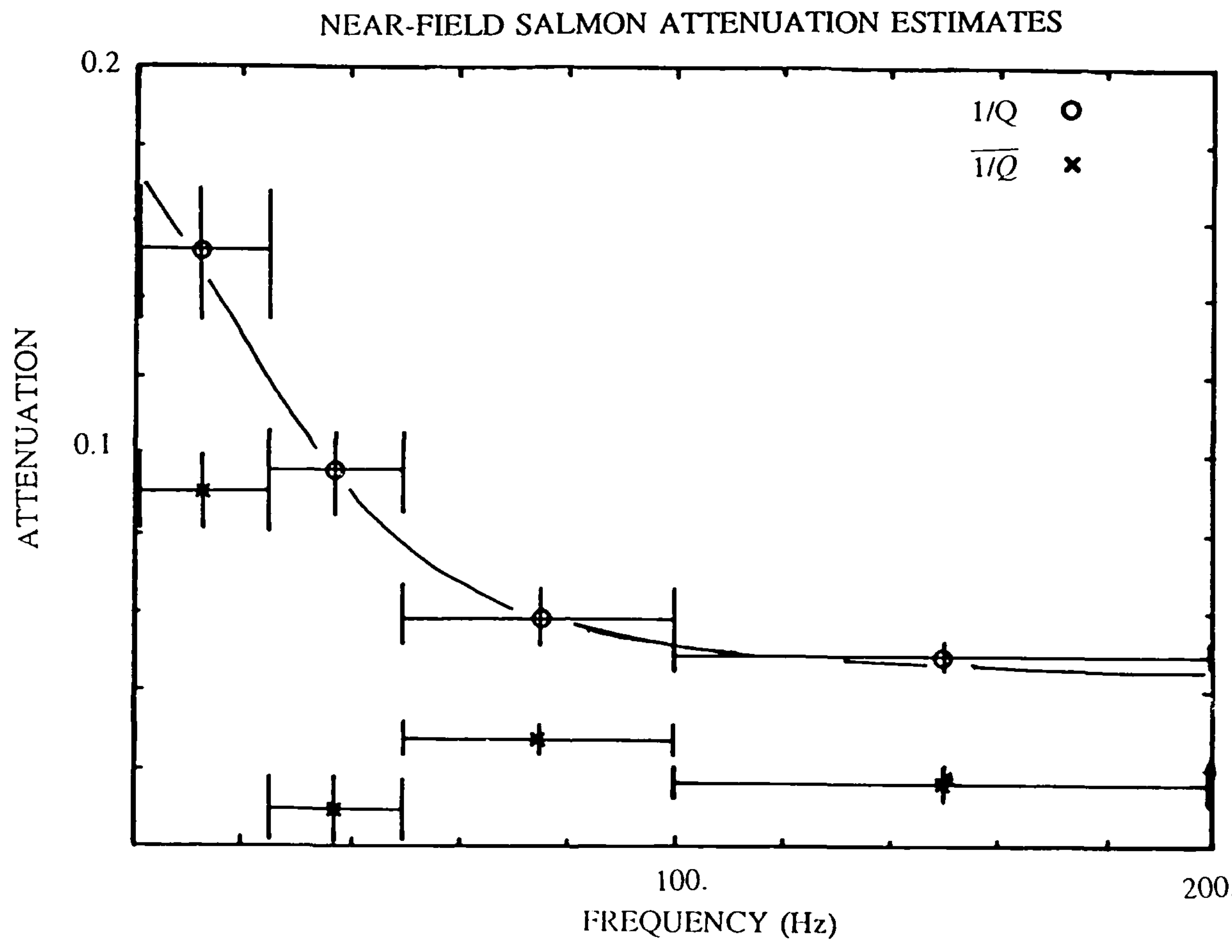

Figure 8. 1/Q and $\overline{1/Q}$ estimates from RVP spectral ratios as a function of frequency bandwidth. A smooth 1/Q(f) curve is drawn through the data consistent with both the average 1/Q values and the slope of 1/Q inferred from $(\overline{1/Q}-1/Q)/f$.

ture of the spectral ratios in Figures 5A, 5B, and 5C require that $\overline{1/Q}$ must be frequency dependent and $1/Q(f)$ must increase with increasing frequency.

TABLE 4. SUMMARY OF AVERAGE FREQUENCY DEPENDENCE (URH)

Freq. Band	f	Q	$\overline{Q}$	1/Q	$\overline{1/Q}$	$(\overline{1/Q}-1/Q)/f$
	1.0	5.76	5.84	0.174	0.171	-0.00211
1-25	13.5	6.79	8.42	0.147	0.119	-0.00211
25-50	37.5	10.5	70.6	0.0952	0.0142	-0.0022
50-100	75.0	17.0	38.6	0.0588	0.0259	-0.00044
1-200.	99.0	21.3	39.1	0.0469	0.0256	-0.00022
100-200.	150.0	25.1	61.8	0.0398	0.0162	-0.00016
	200.0	28.7	162.	0.0348	0.00618	-0.00014

DISCUSSION AND CONCLUSIONS

We see that the Salmon near-field data indicates that the non-linear near-field Q(f, r) increased with increasing frequency and decreasing strain rate. The Sterling linear near-field Q was nearly frequency independent and greater by an order of magnitude. However, to clearly see these relationships it is necessary to average over either distance ranges or frequency bands to attain the respective resolution of 1/Q(f, r) in either the the frequency or spatial domains. While the Sterling data are consistent with the theory of Minster and Day (1986) based on the Cowboy chemical explosions in Salt, the Salmon 1/Q declines at a slower rate, $\approx 1/\sqrt{r}$, than would be expected if the attenuation rate were directly proportional to strain. These two nuclear explosions bracket the Cowboy chemical explosion data modeled by Minster and Day. Another possibility may be consistent with the results of Figure 7, that the attenuation rate changes near 300 meters and is nearly constant for ranges greater than 300 meters. This is roughly coincident with the equivalent elastic radius inferred from the regional P-wave corner frequency.

We see that explosions decoupled in salt may be enhanced in high frequencies over a well coupled shot in salt because of the strain and frequency dependence of near-field attenuation. Springer et al (1968) estimated the decoupling factor of Sterling to be 70(20) at 1 to 2 Hz using surface seismic recording stations. Blandford and Woolson (1979) used regional data to estimate the Salmon/Sterling spectral ratio for P waves to be about 1000 at 1 Hz and only about 17 at 25 Hz. The decline of decoupling at high frequencies becomes a critical factor for detection and discrimination of decoupled shots. In case of the Salmon/Sterling experiments, the differences in near-field attenuation may account for as much as a factor of 2 at 10 Hz, and 5 at 100 Hz, if the proposed Q(f,r) model is valid in the range from 200 to 1000 meters.

REFERENCES

Blandford, R. R. and J. R. Woolson (1979). Experimental spectral analysis of Salmon/Sterling decoupling, *SDAC-TR-79-3*, Teledyne Geotech, Alexandria, Virginia.

Der, Z. A., T. W. McElfresh, and A. O'Donnell (1982). An investigation of the regional variations and frequency dependence of anelastic attenuation in the mantle under the United States in the 0.5-4 Hz band, *Geophys. J. 69*, 67-99.

Evernden, J. F., C. B. Archambeau, and E. Cranswick (1986). An evaluation of seismic decoupling and underground nuclear test monitoring using high-frequency seismic data, *Rev. Geophysics 24*, 143-215.

Hannon, W. J. (1985). Seismic verification of a comprehensive test ban, *Science 227*, 251-257.

Langston, C. A. (1983). Kinematic analysis of strong motion P and SV waves from the Sterling event, *J. Geophys. Res. 88*, 3486-3497.

Larson, D. B. (1979). Spherical wave propagation in elastic media and its application to energy coupling for tamped and decoupled explosions, *UCRL-52655*, Lawrence Livermore Laboratory, Livermore, California.

Minster, J. B. and S. M. Day (1986). Decay of wave fields near an explosive source due to high-strain, nonlinear attenuation, *J. Geophys. Res. 91*, 2113-2122.

McCartor, G. D., and W. R. Wortman (1985). Experimental and analytic characterization of nonlinear seismic attenuation, *MRC-R-900*, Mission Research Corporation, Santa Barbara, California.

Perret, W. R. (1968a). Free-field particle motion from a nuclear explosion in salt, Part 1, *VUF-3012*, Sandia Laboratory, Albuquerque, New Mexico.

Perret, W. R. (1968b). Free-field ground motion study, Project Sterling, *SC-RR-68-410*, Sandia Laboratory, Albuquerque, New Mexico.

Springer, D., M. Denny, J. Healy, and W. Mickey (1968). The Sterling experiment: decoupling of seismic waves by a shot-generated cavity, *J. Geophys. Res. 73*, 5995-6011.

Wortman, W. R., and G. D. McCartor (1985). Analytic approaches to linear and nonlinear attenuation, in *The VELA Program: A Twenty-Five Year Review of Basic Research*, A. U. Kerr, Editor, Defense Advanced Research Projects Agency, Rosslyn, Virginia.

Workman, J. W. and J. G. Trulio (1985). Cowboy Trails: analysis of gauge records for peak velocity and wavespeed, *PAI-FR-0119-2*, Physics Applications Inc., Los Angeles, California.

DISTRIBUTION LIST
FOR UNCLASSIFIED REPORTS
DARPA-FUNDED PROJECTS
(Last Revised: 5 Jan 1987)

RECIPIENT	NO. OF COPIES
DEPARTMENT OF DEFENSE	
DARPA/GSD ATTN: Dr. R. Alewine and Dr. R. Blandford 1400 Wilson Boulevard Arlington, VA 22209-2308	2
DARPA/PM 1400 Wilson Boulevard Arlington, VA 22209-2308	1
Defense Intelligence Agency Directorate for Scientific and Technical Intelligence Washington, D.C. 20301	1
Defense Nuclear Agency Shock Physics Washington, D.C. 20305-1000	1
Defense Technical Information Center Cameron Station Alexandria, VA 22314	12
DEPARTMENT OF THE AIR FORCE	
AFGL/LWH ATTN: Dr. J. Cipar and Mr. J. Lewkowicz Terrestrial Sciences Division Hanscom AFB, MA 01731-5000	2
AFOSR/NPG ATTN: Director Bldg. 410, Room C222 Bolling AFB, Washington, D.C. 20332	1

AFTAC/CA ATTN: STINFO Officer Patrick AFB, FL 32925-6001	1
AFTAC/TG Patrick AFB, FL 32925-6001	3
AFWL/NTESG Kirtland AFB, NM 87171-6008	1

DEPARTMENT OF THE NAVY

NORDA ATTN: Dr. J.A. Ballard Code 543 NSTL Station, MS 39529	1

DEPARTMENT OF ENERGY

Department of Energy ATTN: Mr. Max A. Koontz (DP-52) International Security Affairs 1000 Independence Avenue Washington, D.C. 20545	1
Lawrence Livermore National Laboratory ATTN: Dr. J. Hannon and Dr. M. Nordyke University of California P.O. Box 808 Livermore, CA 94550	2
Los Alamos Scientific Laboratory ATTN: Dr. K. Olsen and Dr. T. Weaver P.O. Box 1663 Los Alamos, NM 87544	2
Sandia Laboratories ATTN: Mr. P. Stokes Geosciences Department 1255 Albuquerque, NM 87185	1

OTHER GOVERNMENT AGENCIES

Central Intelligence Agency ATTN: Dr. L. Turnbull OSI/NED, Room 5G48 Washington, D.C. 20505	1

U.S. Arms Control and Disarmament Agency 1
ATTN: Dr. M. Eimer
Verification and Intelligence Bureau, Rm 4953
Washington, D.C. 20451

U.S. Arms Control and Disarmament Agency 1
ATTN: Mrs. M. Hoinkes
Multilateral Affairs Bureau, Rm 5499
Washington, D.C. 20451

U.S. Geological Survey 1
ATTN: Dr. T. Hanks
National Earthquake Research Center
345 Middlefield Road
Menlo Park, CA 94025

U.S. Geological Survey 1
ATTN: Dr. R. Masse
Global Seismology Branch
Box 25046, Stop 967
Denver Federal Center
Denver, CO 80225

UNIVERSITIES

Boston College 1
ATTN: Dr. A. Kafka
Western Observatory
381 Concord Road
Weston, MA 02193

California Institute of Technology 1
ATTN: Dr. D. Harkrider
Seismological Laboratory
Pasadena, CA 91125

Columbia University 1
ATTN: Dr. L. Sykes
Lamont-Doherty Geological Observatory
Palisades, NY 10964

Cornell University 1
ATTN: Dr. M. Barazangi
INSTOC
Snee Hall
Ithaca, NY 14853

Harvard University 1
ATTN: Dr. J. Woodhouse
Hoffman Laboratory
20 Oxford Street
Cambridge, MA 02138

Massachusetts Institute of Technology 3
ATTN: Dr. S. Soloman, Dr. N. Toksoz, and Dr. T. Jordan
Department of Earth and Planetary Sciences
Cambridge, MA 02139

Southern Methodist University 1
ATTN: Dr. E. Herrin
Geophysical Laboratory
Dallas, TX 75275

State University of New York at Binghamton 1
ATTN: Dr. F. Wu
Department of Geological Sciences
Vestal, NY 13901

St. Louis University 2
ATTN: Dr. O. Nuttli and Dr. R. Herrmann
Department of Earth and Atmospheric Sciences
3507 Laclede
St. Louis, MO 63156

The Pennsylvania State University 1
ATTN: Dr. S. Alexander
Geosciences Department
403 Deike Building
University Park, PA 16802

University of Arizona 1
ATTN: Dr. T. Wallace
Department of Geosciences
Tucson, AZ 85721

University of California, Berkeley 1
ATTN: Dr. T. McEvilly
Department of Geology and Geophysics
Berkeley, CA 94720

University of California Los Angeles 1
ATTN: Dr. L. Knopoff
405 Hilgard Avenue
Los Angeles, CA 90024

University of California, San Diego 1
ATTN: Dr. J. Orcutt
Scripps Institute of Oceanography
La Jolla, CA 92093

University of Colorado 1
ATTN: Dr. C. Archambeau
CIRES
Boulder, CO 80309

University of Illinois 1
ATTN: Dr. S. Grand
Department of Geology
1301 West Green Street
Urbana, IL 61801

University of Michigan 1
ATTN: Dr. T. Lay
Department of Geological Sciences
Ann Arbor, MI 48109-1063

University of Nevada 1
ATTN: Dr. K. Priestley
Mackay School of Mines
Reno, NV 89557

University of Southern California 1
ATTN: Dr. K. Aki
Center for Earth Sciences
University Park
Los Angeles, CA 90089-0741

DEPARTMENT OF DEFENSE CONTRACTORS

Applied Theory, Inc. 1
ATTN: Dr. J. Trulio
930 South La Brea Avenue
Suite 2
Los Angeles, CA 90036

Center for Seismic Studies 2
ATTN: Dr. C. Romney and Mr. R. Perez
1300 N. 17th Street, Suite 1450
Arlington, VA 22209

ENSCO, Inc.
ATTN: Mr. G. Young 1
5400 Port Royal Road
Springfield, VA 22151

ENSCO, Inc. ATTN: Dr. R. Kemerait 445 Pineda Court Melbourne, FL 32940	1
Gould Inc. ATTN: Mr. R. J. Woodard Chesapeake Instrument Division 6711 Baymeado Drive Glen Burnie, MD 21061	1
Pacific Sierra Research Corp. ATTN: Mr. F. Thomas 12340 Santa Monica Boulevard Los Angeles, CA 90025	1
Rockwell International ATTN: B. Tittmann 1049 Camino Dos Rios Thousand Oaks, CA 91360	1
Rondout Associates, Inc. ATTN: Dr. P. Pomeroy P.O. Box 224 Stone Ridge, NY 12484	1
Science Applications, Inc. ATTN: Dr. T. Bache, Jr. P.O. Box 2351 La Jolla, CA 92038	1
Science Horizons ATTN: Dr. T. Cherry and Dr. J. Minster 710 Encinitas Blvd. Suite 101 Encinitas, CA 92024	2
Sierra Geophysics, Inc. ATTN: Dr. R. Hart and Dr. G. Mellman 11255 Kirkland Way Kirkland, WA 98124	2
SRI International ATTN: Dr. A. Florence 333 Ravensworth Avenue Menlo Park, CA 94025	1
S-Cubed, A Division of Maxwell Laboratories Inc. ATTN: Dr. S. Day P.O. Box 1620 La Jolla, CA 92038-1620	1

S-Cubed, A Division of | 1
Maxwell Laboratories Inc.
ATTN: Mr. J. Murphy
11800 Sunrise Valley Drive
Suite 1212
Reston, VA 22091

Teledyne Geotech | 2
ATTN: Dr. Z. Der and Mr. W. Rivers
314 Montgomery Street
Alexandria, VA 22314

Woodward-Clyde Consultants | 2
ATTN: Dr. L. Burdick and Dr. J. Barker
556 El Dorado St.
Pasadena, CA 91105

NON-U.S. RECIPIENTS

National Defense Research Institute | 1
ATTN: Dr. O. Dahlman
Stockholm 80, Sweden

Blacknest Seismological Center | 1
ATTN: Mr. P. Marshall
Atomic Weapons Research Establishment
UK Ministry of Defence
Brimpton, Reading RG7-4RS
United Kingdom

NTNF NORSAR | 1
ATTN: Dr. F. Ringdal
P.O. Box 51
N-2007 Kjeller
Norway

OTHER DISTRIBUTION

To be determined by the project office | 9